Interfacial welding and reprocessing of engineering thermosets based on surface depolymerization

Xiaojuan Shi[1, 2], Chaoqian Luo[2], Haibao Lu[1, *], Kai Yu[2, *]

1. National Key Laboratory of Science and Technology on Advanced Composites in Special Environments, Harbin Institute of Technology, Harbin, 150080, PR China

2. Department of Mechanical Engineering, University of Colorado Denver, Denver, CO 80217, USA

* Corresponding author HBL: luhb@hit.edu.cn; KY: kai.2.yu@ucdenver.edu

Abstract:

Welding and reprocessing of engineering thermosets are difficult for conventional techniques due to their permanently crosslinked networks. In this study, an interfacial welding method is developed for the anhydride-cured engineering epoxy based on surface depolymerization. The material is first soaked in an alcohol solvent mixed with the catalyst for bond exchange reactions. During the interfacial welding at high temperatures, the solvent molecules break the polymer chains into short segments, which leads to the surface materials being partially depolymerized. The chain segments subsequently disentangle from the network and reconnect on the interface. Assisted by a microscale chemomechanics model, the influences of various processing and material properties are investigated, including the soaking time, welding time, welding temperature, and catalyst content. The parametric studies also reveal welding domains that are respectively dominated by the welding time and soaking time, which provide guidelines to select optimal processing conditions for the practical engineering applications of the welding method. Finally, the welding method is extended to reprocess the epoxy scarps from the powder state. The reprocessed samples are shown to exhibit comparable mechanical properties as the unprocessed ones.

Keywords: *Interfacial welding, repairing, reprocessing, bond exchange reaction, thermosetting polymer.*

1. Introduction

Thermosetting polymers with covalently crosslinked networks are widely used in high-performance engineering applications that require superior chemical resistance and stable thermomechanical properties [1, 2]. However, due to their permanently crosslinked networks, thermosetting polymers are difficult to be reprocessed and recycled using conventional techniques, leading to ever-increasing polymer wastes released into the environment.

There is growing interest to explore interfacial welding methods for thermosetting polymers, which will enable the self-healing capability of the materials, provide alternative approaches to assemble or repair thermoset structures without using glue, and effectively reprocess and recycle polymer wastes. To enable the welding of thermosets and their composites, a widely used method is hybrid welding [3-6], wherein the thermosets or their composites are coated with a thermoplastic film during the material synthesis. The thermoplastic film partially penetrates in the network, leading to mechanical interlocking as the main connection mechanism between the thermoplastic film and the underlying thermoset. The thermosets with the thermoplastic modified surface can be assembled by welding at high temperatures, wherein the welding strength originates from the inter-diffusion and entanglement of linear thermoplastic polymer chains across the interface.

The second technique leverages the interfacial welding effect of dynamic polymers with reversible covalent bonds on the chain backbone, which enables a more efficient, repeatable, and robust repairing of thermosetting polymers. With a given stimulus (*e.g.*, heat, light, or moisture), the reversible bonds break and reform at different rates, leading to the cleavage and reconnection of macromolecular chains in the rearrangeable networks. Recently, bond exchange reactions (BERs) are utilized for the design of dynamic thermosets [7-14], which involve a chain connection followed immediately by a chain cleavage to maintain the overall network chain density. Various dynamic chemistry can be employed for BERs, such as the light-sensitive reversible addition-fragmentation transfer [15, 16], thermal-sensitive transesterification [17, 18], transamination of vinylogous acyls [19, 20], transcarbamoylation [21, 22], transalkylation [23], imine exchange [14, 24-28], and disulfide exchange [29, 30]. Comprehensive summaries of existing dynamic chemistry for CANs can be found in recent

reviews [31-33]. Overall, when two pieces of dynamic thermosets are brought into contact, cleaved polymer chains will be reconnected on the interface due to BERs, which lead to robust welding with interfaces connected primarily by covalent bonds [34-50]. In addition, the welding process does not require reactive regent within the network and thus can be repeated multiple times.

CANs are often elastomeric networks at room temperature because they are built from monomers or hardeners with flexible structures to ensure the high mobility of the network. Recently, there is growing interest to develop tough CANs with higher glass transition temperatures (T_g), so they can be applied as load-bearing structural materials in high-performance engineering applications. For example, Liu et al. [51] synthesized epoxy CANs using a bio-based tri-functional epoxy monomer with network T_g up to 187 °C. Giebler et al. [52] prepared CANs from tetra- and tri-functional epoxy monomers using glutaric anhydride as the hardener. The network exhibited a T_g around 140°C. It showed remarkable stress relaxation when the temperature was above 200°C, enabling the reprocessing and recycling of the materials.

Despite the exciting developments of CANs, most of them are designed and synthesized in an *ad hoc* manner with specific dynamic bonds built in the networks, and a proper selection of catalysts is required. It is in high demand to explore if the interfacial welding and reprocessing mechanisms of CANs can be extended to the general engineering thermosets, which feature permanently crosslinked networks without BER capability and are currently making up the bulk of recycling problems.

In this paper, we develop an interfacial welding technique for the repairing and reprocessing of engineering thermosets based on surface depolymerization. Compared to our previous works on material reprocessing that use vitrimers as the material platform [26, 50, 53-57], this study employs an anhydride-cured engineering epoxy without BER capability. The welding process involves two steps. First, the epoxy sample is soaked in an alcohol solvent mixed with the catalyst for transesterification BERs at a relatively low temperature. Both constituents gradually diffuse into the polymer. Second, after soaking, two pieces of epoxy samples are brought into contact at a relatively high temperature. The solvent

molecules participate in transesterifications with ester bonds on the chain backbone, which break the polymer chains into short segments [54, 55, 58] and lead to surface depolymerization. The cleaved chain segments subsequently disentangle from the network onto the interface and reconnect through reverse BERs with the generated solvent molecules evaporating out of the system. The welding strength increases with the amount of polymer chains connected on the interface.

This new technique leads to the welding of engineering epoxy with covalent bonding on the interface. A multiscale chemomechanics theoretical model is defined in this work to capture the experimental results on the welding strength at different soaking times and welding times. It is applied to unravel the influencing mechanisms of different processing conditions, such as the welding temperature and catalyst content, and reveal welding domains that are respectively dominated by the welding time and soaking time. The fundamental understanding is further extended to reprocess epoxy wastes from the powder state. The influences of soaking time and welding time on the mechanical strength of reprocessed samples are investigated. While the anhydride-cured epoxy is used as the material platform in this work, the welding technique is expected to be extended to the repairing of other ester-containing thermosets, such as polyester, vinyl ester, and polyurethane, which were reported to share 71% of the global thermoset resin market in thermoset industry [59].

2. Materials and Experiments

2.1 Material synthesis and overall welding process

The anhydride-cured epoxy samples were synthesized using the epoxy monomer (poly-bisphenol A-co-epichlorohydrin, glycidyl end-capped, Mw=1075 g/mol) and Hexahydro-4-methylphthalic anhydride (Mw=168 g/mol) as the crosslinker. Both chemicals were purchased from Sigma Aldrich (St. Louis, MO, USA) without further purification. During the synthesis, 100 parts by weight of the epoxy monomer and 31.25 parts by weight of crosslinker were first mixed in a round-bottom flask and manually stirred until the mixture became homogeneous. The molar ratio between the epoxide group and anhydride was 1:1.

Then, the mixture was poured into a mold and cured in an oven for 15 hours at 150°C. The synthesized network was shown to exhibit a glass transition temperature (T_g) of 64.5°C [60].

Note that adding an accelerator will greatly promote the curing speed of the epoxy networks. In the Supplementary Materials (Section S1), an epoxy sample was synthesized using the same amount of epoxy monomer and crosslinker. In addition, 0.375 part by weight of accelerator (4,6-tris-dimethylaminomethyl phenol) was added. The mixture was first pre-cured at 100 °C for 2 h and then post-cured at 150 °C for another 2 h. It shows that the transition temperature T_g of the network without accelerator (64.5^{o}C) is very close to that of network with accelerator (69.6 ^{o}C). The network rubbery modulus, which scales to the crosslinking density, is also close to each other. The close comparison suggests that the epoxy networks used in this study are fully cured without significant unreacted or products of side reactions.

The anhydride-cured epoxy contains ester groups on the chain backbone (Fig. 1a), which react with the hydroxyl groups of alcohol solvent molecules *via* transesterification. The overall welding process is shown in Fig. 1b. The epoxy samples were first soaked in ethylene glycol (EG) solvent mixed with the catalyst for transesterification BERs (triazabicyclodecene, TBD). In this work, ethylene glycol is used for interfacial welding and reprocessing because it is a small-molecule solvent (62g/mol) with a relatively higher diffusivity compared to other high-molecule solvents. Also, it has two hydroxyl groups in each molecule, which would promote the rate of the transesterification BERs during the reprocessing. More rigorous studies are needed in the future to consider the interaction parameters between the solvent and epoxy networks for the selection of optimal processing conditions, such as recent studies based on the Hansen theory [61, 62].

After soaking for a given time, the samples were taken out, and the solvent on the sample surface was carefully wiped off. They were brought into contact at high temperatures for surface welding. The zoom-in presentation shows the breaking and reconnection of polymer chains *via* transesterification BERs, which respectively occur within the network and on the sample interface. After being welded for a given time, lap-shear tests were performed to examine the welding strength.

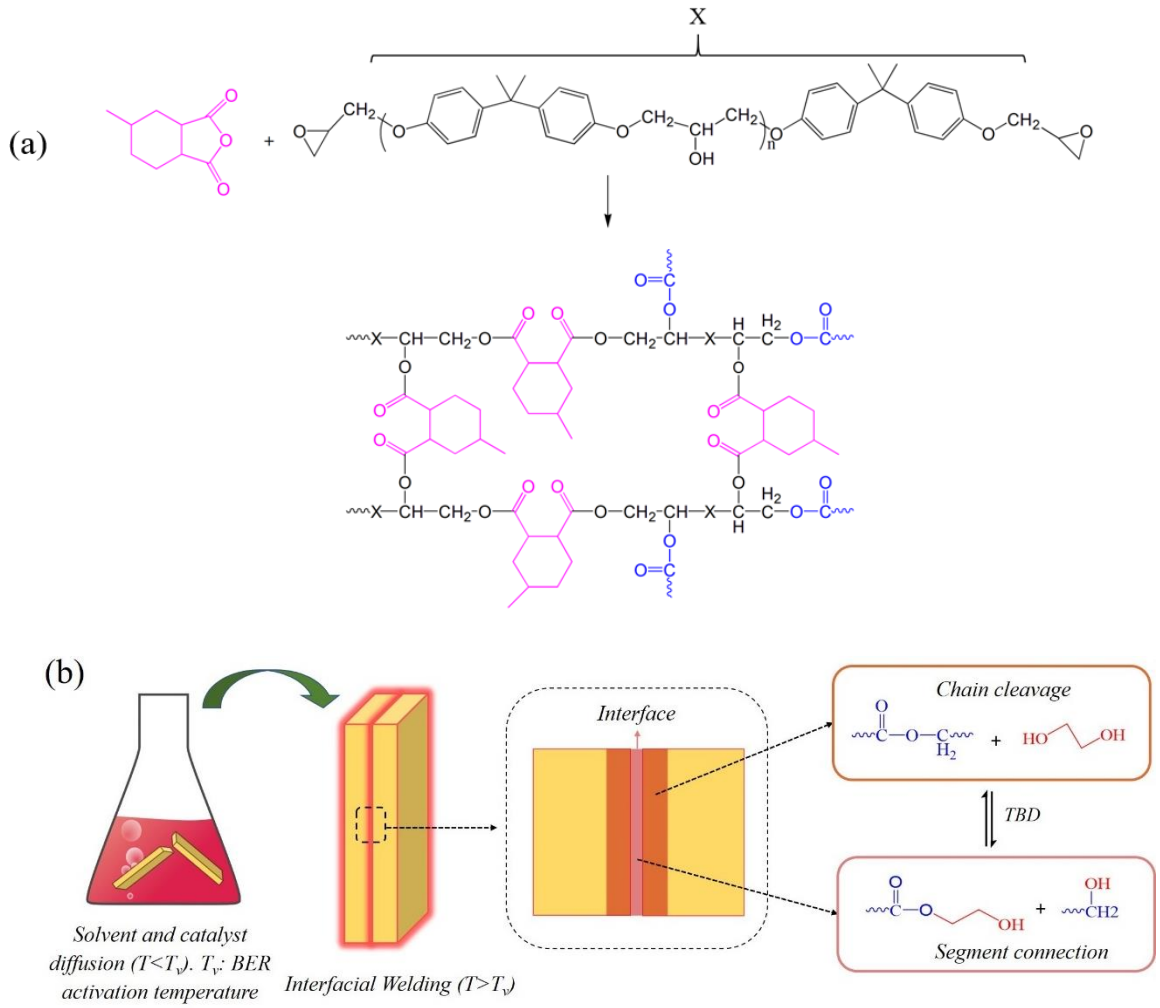

Fig. 1. (a) Schematic view showing the synthesis of anhydride-cured epoxy. The network contains ester bonds on the chain backbone, which can react with hydroxyl groups of solvent molecules *via* transesterification BERs; **(b)** The overall view of the welding process. The sample is first soaked in the alcohol solvent mixed with BER catalyst. During the subsequent welding, the polymer chains within the network are cleaved into short segments, which disentangle from the material and reconnect on the interface. Zoom-in views showing the cleavage and reconnection of ester bond on the chain backbone.

2.2 Identification of appropriate soaking and welding temperature

When soaking the epoxy sample in the alcohol solvent mixed with the BER catalyst, the small molecules are expected to diffuse into the network, primarily concentrating around the sample surface. If the soaking temperature or the catalyst content is too high, the polymer

chains on the epoxy surface will be quickly cleaved into segments and disentangle out from the network. This essentially leads to material degradation in the solvent, which is undesirable for the subsequent welding. The appropriate soaking and welding temperatures are identified using swelling tests, Fourier Transform Infrared Spectroscopy (FTIR) measurements, and stress relaxation tests on epoxy samples.

To identify a proper soaking condition to enable effective diffusion while avoiding notable network depolymerization, epoxy samples were cut into the same dimension (10 mm × 10 mm × 1 mm) and soaked in ~3g solvent in a beaker with different contents of catalyst. The beaker was covered with a glass lid and placed in an oven for temperature control. At times, the sample was taken out from the solvent, and the mass was measured after wiping the surface.

FTIR tests were performed on epoxy samples with ~0.1 mm thickness. If the sample was in the viscous liquid state, it was sandwiched between two salt crystals. The spectra were recorded on a Nicolet iS50 FTIR spectrometer (Thermo Scientific, Waltham, MA, USA) by averaging 32 scans of the signal at a resolution of 2 cm^{-1}.

The stress relaxation tests were conducted using the Dynamic Mechanical Analysis (DMA, Model Q800, TA Instruments, New Castle, DE, USA) tester in tension state. The epoxy samples were cut into the same dimension (10 mm in length, 3 mm in width, and 0.8 mm in thickness). During the tests, the strain amplitude was set to be 5%, and the stress relaxation time was set to be 40 min for all cases. The drop in stress was recorded to calculate the relaxation modulus.

2.3 Measurements of interfacial welding kinetics

In this work, the lap-shear tests are adopted to examine the interfacial shear strength of welded epoxy with different welding times. The epoxy samples were first cut into a uniform dimension (1 mm × 5 mm × 20 mm) and immersed in the EG solvent mixed with TBD for a period. As will be shown in the Results Section, a soaking temperature of 80^{o}C was selected and the soaking time ranged from 10-120 mins. Further increasing the temperature could enhance the solvent diffusion, but it will lead to active BERs and material decomposition

over an extended soaking time.

The samples were then taken out and wiped using tissue paper until no visible liquid is attached to the surface. Fig. 2a shows the schematic view of the sample preparation process, as well as the sample dimensions. Fig. 2b shows the appearance of the welded sample. In this pilot study, the sample dimensions for lap-shear tests do not follow the ASTM standard. The reported data aims to demonstrate the feasibility of the welding method and reveal its working mechanism with different processing variables. Lap-shear tests may need to be performed following a standard (e.g., ASTM D1002) in the future for a more rigorous comparison with other literature data.

The two pieces of samples were brought into contact with an interfacial contact area of 25 mm^2. An equivalent welding pressure of 0.5 MPa was applied, which was realized by applying a controlled force over the welding region using the MTS tester. As shown in Fig. 2a, to prevent the fracture of epoxy sample in the tensile direction during the lap-shear tests, aluminum alloy films (~0.3 mm) were bounded on the sample surface using a superglue. This will ensure the lap-shear samples already break from the interface during the tests. Note that the welding pressure may affect the rate of BERs and thus the welding kinetics. As shown in the previous work [63, 64], high pressure may enhance the rate of chain cleavage at equivalent temperatures during the BERs. In this work, the welding pressure is identical for all lap-shear tests, and it is moderate, only serving to maintain good contact between the two samples. The welding time ranges from 10 mins to 120 mins at 100 °C. After welding, the component was subject to the lap shear tests at room temperature to measure the interfacial shear strength. The tests were performed on the MTS machine (Model Insight 10, Eden Prairie, MN, USA). The interfacial shear stress was taken to be the axial force divided by the overlapping area.

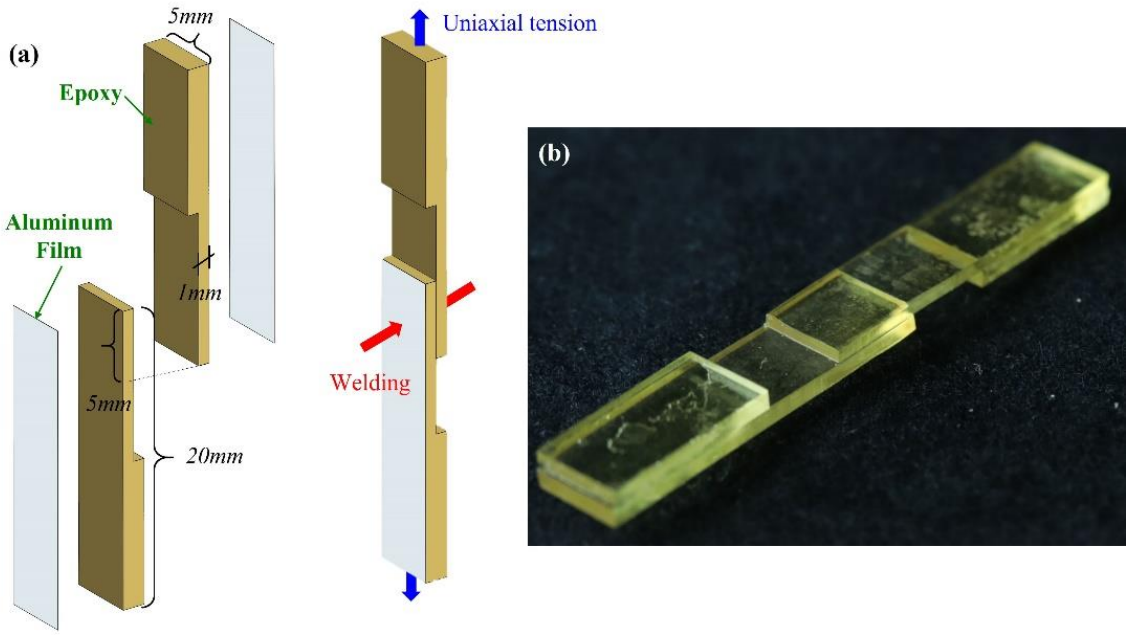

Fig. 2. (a) A schematic view of the sample preparation for lap-shear tests. A thin aluminum film is attached to the epoxy sample to avoid its failure in the tension direction. **(b)** A welded sample used for the lap-shear test (without attaching the aluminum film to give a better view).

2.4 Reprocessing epoxy waste from the powder state

The interfacial welding of the epoxy sample was extended in the microscale to reprocess the epoxy sample from the powder state. Bulk samples were first manually ground on sandpaper. The powder was collected and immersed in the EG solvent mixed with the catalyst for different times. Subsequently, the powder was filtered out and transferred into an aluminum mold to be heated at 100^{o}C on the MTS machine. A 0.5 MPa pressure was applied to ensure good contact among the epoxy particles. It should be noted that the pressure was small and would not notably affect the rate of transesterification reactions [65-67]. After being heated for a given time, the polymer power was welded into a solid sample. The uniaxial tension tests of reprocessed samples were followed at room temperature to examining the welding strength. The tests were performed using the Electro-Force Dynamic Mechanical Analyzer (DMA, TA Instruments, Model 3230). Rectangular samples were cut into a uniform geometry (57 mm in length, 13 mm in width, 2.5-3.0mm in thickness) for testing. The sample dimension is essentially the middle section of the Type 1 tension sample in ASTM 638-14 standard.

3. Constitutive Modeling Framework

3.1 Diffusion of solvent and catalyst small molecules

Before surface welding, the epoxy samples are soaked in the solvent mixture. A relatively low temperature is selected so the BERs within the network are negligible. The transportation of solvent molecules in the epoxy network can be described using Fick's laws of diffusion:

$$\frac{\partial C_{eg}}{\partial t} = D_s\left(T\right)\frac{\partial^2 C_{eg}}{\partial x^2}. \tag{1}$$

In the above equation, C_{eg} is the volume mole content of EG solvent. D_s is the molecular diffusivity. Its temperature dependency follows the Arrhenius equation:

$$D_s\left(T\right) = D_0 \exp\left(-\frac{E_{as}}{RT}\right). \tag{2}$$

where D_0 is the reference diffusivity, E_{as} is the diffusion activation energy, R is the gas constant. D_0 and E_{as} can be readily determined by performing swelling tests on the epoxy samples at different temperatures. The BER catalyst acts as a solute and is carried into the network by the alcohol solvent. Note that the transportation of different chemicals in the polymer networks may depend on their interaction parameters. In this work, for the convenience of analysis, we assume that the mole ratio between the catalyst and EG solvent molecules within the network is the same as that in the solvent mixture.

3.2 Interfacial welding kinetics and shear strength

During surface welding, a relatively high temperature is used to activate the BERs. Within the epoxy network, the extensive number of solvent molecules drives the reaction equilibrium in Fig. 1b to the direction of chain cleavage. The average chain segment length gradually decreases. On the sample interface, the generated solvent molecules can quickly evaporate, so the reaction equilibrium shifts to the direction of chain connection with increasing segment length.

The mechanism of solvent-assisted interfacial welding is presented in Fig. 3. The overall welding process is split into three steps for the modeling purpose: first, the polymer chains around the sample surface are cleaved by EG molecules *via* transesterification BERs. Second,

the short chain segments of various lengths disentangle from the network at a rate proportional to the segment length. These segments gradually accumulate on the interface. Third, the chain segments on the interface reconnect *via* reverse transesterification. The generated solvent molecules evaporate from the interface. In terms of this, the density of connected polymer chains on the interface gradually increases, which results in the promoted welding strength.

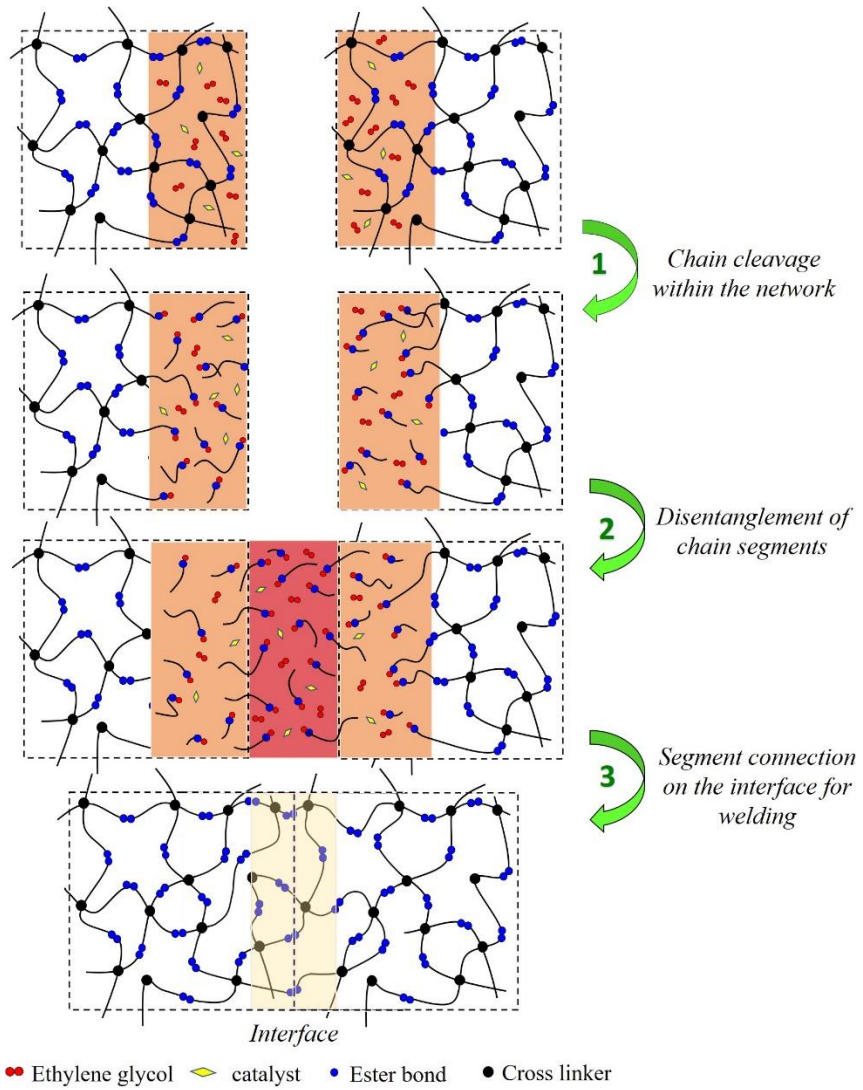

Fig. 3. A schematic representation of the welding process. Note that the interfacial welding region is enlarged for the purpose of better visualization.

Step 1: chain cleavage within the network: Herein, the microscale reaction rate between solvent molecules and polymer chains is formulated based on our previous work [56]. For the chain cleavage reaction, the solvent molecules first disuse towards the ester bonds on the

chain backbone and then break the chain *via* BER. The chain cleavage rate, k_1 (*mol/s*), is written as:

$$k_1 = \left(N_A t_1 + N_A t_{BER}\right)^{-1}, \tag{3}$$

where N_A is the Avogadro's number (6.02×10^{23} mol^{-1}), $t_1 = \langle r_1 \rangle^2 / D_s$ is the traveling time of the solvent molecule, with $\langle r_1 \rangle$ being its average distance towards an ester bond. According to the theory of mean inter-particle distance, $\langle r_1 \rangle = 1/3\, \Gamma(1/3) a$, where Γ is the gamma function, and $a = \sqrt[3]{4 N_A \pi C_{eg}/3}$, is the Wigner-Seitz radius. $t_{BER} = t_{0_{BER}} \exp(E_a/RT)$, is the average time spent on a BER, with E_a being the BER energy barrier, and $t_{0_{BER}}$ being a time constant.

For the chain connection, the chain segments diffuse towards another reactive site at the segment tails and then connect *via* reverse BERs. The reaction rate, k_2 (*mol/s*), is written as:

$$k_2 = \left(N_A t_2 + N_A t_{BER}\right)^{-1}, \tag{4}$$

where $t_2 = \tau_i (C_r N_A b^3)^{-\frac{4}{3}}$, is the traveling time of a segment with i monomers, with C_r being the concentration of reactive site at the chain tails at a continuum point, and b being the monomer length. τ_i is the Rouse time of chain segment with i monomers. As shown in Supplementary Materials (Section S5), $\tau_i = \tau_0 i^2 \alpha(T)$, with τ_0 being the Rouse time of the shortest segment, and $\alpha(T)$ being the shift factor for time-temperature superposition principle.

The chain connection rate (k_1) and cleavage rate (k_2) are then used in first-order reaction equations to formulate the content and length distribution of chain segments within the epoxy networks. There are four types of exchange reactions that can change the mole content of chain segments with i monomers (*i.e.,* C_i). As illustrated in Fig. S1 (Supplementary Materials, Section S2), the four reactions are: (a) a segment with i monomers breaks into shorter segments after reacting with an EG molecule; (b) a segment with i monomers connects with another segment to form a longer one; (c) two short segments connect to form a segment with i monomers; and (d) a long segment react with an EG molecule to form a segment with i monomers and another short segment. The changing rate of C_i is the summation of the reaction rates of the four reactions:

$$\dot{C}_i = \underbrace{-k_2 C_i}_{r_a} \underbrace{-k_1 C_i}_{r_b} + \underbrace{k_1 \sum_{j=1}^{i-1} C_j \left(C_{i-j} \Big/ \sum_m C_m \right)}_{r_c} + \underbrace{k_2 \sum_{j=i+1} C_j \left(2/(j-1) \right)}_{r_d}, \tag{5}$$

<u>*Step 2: Disentanglement of chain segments:*</u> After the polymer chains are cleaved into shot segments, they disentangle from the epoxy network and present on the interface. According to the reptation theory [68, 69], the segment disentanglement rate, r_{di} ($mol/m^3 s$), is scaled to the segment length and is formatted as:

$$r_{di} = \alpha_d \frac{C_i}{\tau_i}, \tag{6}$$

where α_d is a scaling factor. τ_i is the Rouse time (Eq. 4) of segments with i monomers.

<u>*Step 3: Connection of chain segments on the interface for welding:*</u> For the chain connection on the interface, the evolution of segment contents still follows Eq. 5. Due to the solvent evaporation boundary condition, the chain connection rate k_2 is much higher than the chain cleavage rate k_1, so the average chain segment length increases. The reaction kinetics can be determined based on the solvent evaporation rate, k_d.

After two segments are connected, an ester bond will be formed on the backbone. Therefore, the amount of connected segments equal to the amount of ester bonds on the interface, which is $\sum_{i=2}(i-1)C_i(t)$. An interfacial welding degree parameter, Q, can be defined to be the content of ester bonds on the interface normalized by its initial value in the fully polymerized network:

$$Q(t) = \frac{\sum_{i=2}(i-1)C_i(t)}{(N-1)C_N}, \tag{7}$$

In the above equation, N is the number of monomers along the chain backbone in the unprocessed epoxy sample, which are separated by N-1 ester bonds. C_N is the mole content of polymer chains. Both parameters can be determined based on the stoichiometry during the material synthesis.

Q is essentially a scalar varies between zero to one. Q=1 suggests that all the chain segments are fully connected, and the interfaces are completely welded. Following the previous studies [50, 70], the macroscale interfacial shear strength is proportional to the welding degree. Overall, using Eqs. 1-5, one can determine the chain segment length

distribution within the network (close to the sample surface). The calculations are then fed into Eq. 6 to determine the amount and length distribution of chain segments disentangled from the network and diffused onto the interface. These calculations are finally submitted into Eq. 7 to determine the interfacial welding degree, Q, which is used to compare with the experimental data of the normalized shear strength.

3.3 Identification of material parameters

All the material parameters can be calculated or determined by standard polymer tests. For example, the diffusivity parameters in Eq. 2 were determined by performing swelling tests on the epoxy samples at different temperatures. As shown in Fig. S3 (Supplementary Materials, Section S3), when the diffusion coefficient E_{as} = 2.68 *kJ/mol* and the pre-factor D_0 = 1.5×10^{-2} mm^2/s, the model predictions agree well with the experimental data. The solvent evaporation rate (k_d) for interfacial chain connection was determined by measuring the mass loss of pure EG solvent at different temperatures (Supplementary Materials, Section S4). In our previous work [56, 71, 72], the BER activation energy E_{ab} was measured by performing a series of stress relaxation tests on the as-fabricated epoxy samples to determine the relaxation times at different temperatures. All the material parameters and their associated identification methods are described in the Supplementary Materials (Section S5).

4 Results and Discussion

4.1 Determining a suitable soaking temperature

To enable the successful welding of epoxy, it is critical to select appropriate soaking and welding conditions. Ideally, during the soaking process, a moderate temperature should be used such that both alcohol solvent and catalyst can effectively diffuse into the network, but the BERs are negligible due to the relatively low temperature. An excessive soaking temperature would lead to network decomposition and material loss, which is unwanted for the subsequent welding. During the interfacial welding process, a relatively high temperature will be used to enable active BERs between alcohol solvent and network, which break the polymer chains at the position of ester bonds. This process is reversible. If the solvent quickly

evaporates on the interface, the cleaved polymer chains will be reconnected on the interface with ester bonds reformed on the backbone.

To identify the optimal processing conditions, we start with swelling tests on the epoxy sample to examine the influences of soaking temperature and catalyst content on the material mass. Fig. 4 shows the change of normalized mass of the epoxy sample in EG solvent as a function of heating time at different temperatures and TBD contents. It is observed that at temperatures above 100°C, the sample quickly lost the mass from the beginning in the EG solvent with 1 wt% TBD catalyst, which suggests active BERs between the solvent molecules and epoxy networks. At 180°C, the sample is fully depolymerized into soluble monomers within ~60 mins. Decreasing the temperature reduces the rate of BERs and thus the mass dropping rate. When the temperature is decreased to 80°C, there is no significant depolymerization observed, and the mass loss after soaking is only ~2 wt% after 140 mins. With the same soaking temperature, we further decrease the catalyst content to be 0.1 wt%. The mass of epoxy is seen to be increased, which suggests swelling of solvent modules of the epoxy network, but negligible disentanglement of chain segments into the solvent.

Based on these observations, we choose to use the EG solvent containing 0.1 wt% TBD to soak the epoxy samples at 80°C. For the interfacial welding, the temperature is set to be 100°C or higher to enable effective BERs between the EG solvent and epoxy networks.

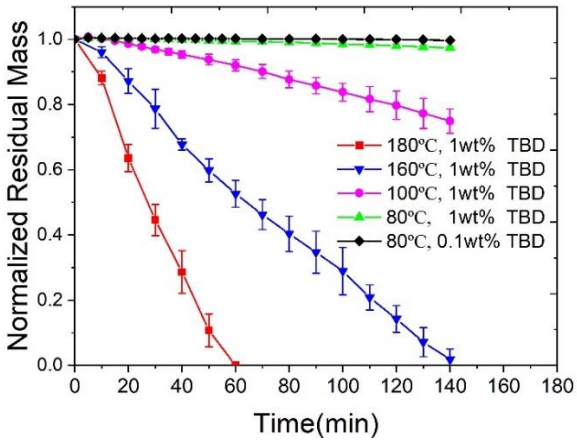

Fig. 4. Normalized residual mass of the epoxy sample in EG solvent as a function of heating time with different temperatures and TBD contents.

FTIR measurements were performed to confirm that the welding process would work as expected at the selected soaking and welding temperatures. Four measurements were performed, and the testing results are shown in Fig. 5. In the first measurement (Fig. 5a), a fresh, as-prepared epoxy sample was tested as the reference. The spectrum shows a signature absorption peak of ester at 1730 cm^{-1}. In the second measurement (Fig. 5b), the epoxy sample was immersed in ethylene glycol solvent at 80^{o}C for 20 mins. The FTIR measurement suggests that there is no notable difference in the ester absorption peak, but an increased absorption peak of the hydroxyl group at ~3300 cm^{-1}, which proves the diffusion of solvent molecules into the network. In the Supplementary Materials (Section S6), stress relaxation tests were performed on this sample at 80^{o}C. The results suggest that after soaking, the solvent molecules do not react with the network due to the relatively low temperature and inactive BERs. Most solvent molecules would isolate within the network.

In the third measurement (Fig. 5c), the epoxy sample was soaked in 100^{o}C ethylene glycol solvent for 2 hours until it is fully decomposed in the solvent. Then the decomposition solution was poured into water and stabilized at room temperature for 12 hours until phase separation, wherein the anhydride derivatives are water-soluble, and the derivatives of epoxy monomers are not water-soluble. After precipitates, the epoxy derivatives were separated and subject to FTIR measurements. It can be observed that the characteristic peak of ester moieties almost disappeared in the recycled epoxy derivatives, indicating complete elimination of ester moiety. This result indicates that at 100^{o}C, the transesterification BERs are active to break the polymer chains from the positions of ester bonds.

In the fourth measurement (Fig. 5d), the depolymerized polymer solution was heated at 100^{o}C overnight to evaporate the solvent. The epoxy network is re-polymerized and then subject to the FTIR measurements. The spectrum is close to the fresh reference network with a notable absorption peak of ester. This means that at 100^{o}C and with solvent evaporation boundary conditions, the cleaved polymer chains can be re-connected with ester bonds reformed on the backbone. Overall, the comparisons of the FTIR measurements confirm that the selected soaking temperature and welding temperature would lead to successful welding of epoxy following the mechanism described in the modeling framework.

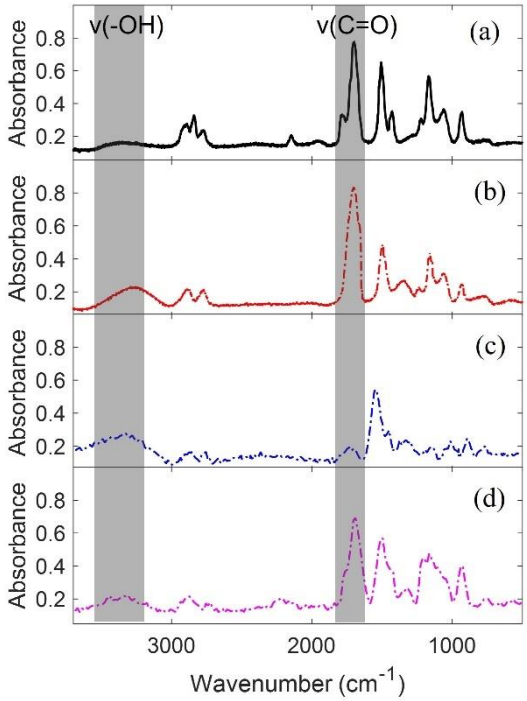

Fig. 5. FTIR spectra of **(a)** a fresh epoxy sample, **(b)** a fresh epoxy sample after soaking in 80oC ethylene glycol for 20 min, **(c)** recycled epoxy derivatives, and **(d)** re-polymerized epoxy sample.

4.2 The shear strength of the welded epoxy sample

Lap-shear epoxy samples (Fig. 2) were prepared to examine the surface welding kinetics. The initial soaking time and the subsequent welding time at 100^{o}C were chosen as the variables. After welding, the mechanical strength of the welded components was examined using the uniaxial tension tests at room temperature, wherein the interfacial shear stress was calculated based on the contact area. Please note that during the initial soaking process, the soaking time and temperature were controlled such that the solvent only slightly diffused into the network close to the sample surface. We do not expect a considerable amount of solvent molecules transported deep into the network. Therefore, the mechanical performance of the bulk epoxy after welding would not be affected notably.

In the Supplementary Materials (Section S7), Fig. S7a shows that for the same soaking time (30 mins), the interfacial shear strength of the sample, which is taken to be the maximum shear stress before interface fracture, increases monotonically with the welding time. It increases from 0.43 MPa at 10 mins of welding to 2.94 MPa at 80 mins of welding. The promoted bonding strength results from the increased amount of polymer chains

connected on the interface. On the other hand, Fig. S7b shows that with the same welding time (80 mins), the interfacial shear strength of the sample also increases with the soaking time. This is because an extended soaking time will lead to more solvent molecules and catalyst diffusing into the network, which promotes the chain cleavage reactions rate (Eq. 3). The polymer chains can rapidly break into short segments with higher diffusivity, and then easily disentangle from the network for interfacial welding [50, 73].

Table 1 summarizes the evolution of interfacial shear strength with the soaking time (from 10 mins to 120 mins) and the welding time (from 10 mins to 80 mins). From the table, it is observed that the welding strength can be promoted by increasing either soaking time or welding time, which suggests their equivalence in promoting the interfacial bonding. It is also observed that as the soaking time increases, the interfacial shear strength of the material increases faster with the welding time. For example, with 120 mins of soaking, the shear strength reaches the maximum value (~ 4.6 MPa) after ~20 mins of welding. While it takes ~70 mins to reach the maximum shear strength when the soaking time is 60 mins. With a soaking time less than 50 mins, the final shear strength could also reach the maximum value with a sufficient welding time provided.

Note that the highest interfacial shear strength, ~4.6MPa, is notably lower than the value achieved using other techniques, such as the hybrid welding of thermoset composites [3], ultrasonic welding of thermoplastic composites [74]. For example, in the hybrid welding of epoxy composites studied by Lionetto et al. [3], the shear strength of welded composites reaches 22.4 MPa for induction welding and up to 27.9 MPa using ultrasonic welding. The reason is that in the presented welding method of thermosets, the welding strength mainly originates from the connected polymer chains on the interface *via* BERs. But for the hybrid welding of thermoset composites or ultrasonic welding of thermoplastic, the processes involve inter-diffusion and entanglement of linear polymer chains around the interface. The chain entanglements could play a more prominent role in the enhancement of interfacial strength compared to the chain connections.

Table 1. The interfacial shear strength of welded epoxy sample under different soaking time and welding time. The maximum values are highlighted in yellow boxes.

		Welding Time (min)				
		10	**20**	**40**	**60**	**80**
Soaking Time (min)	**10**	0.31±0.09	0.42±0.18	0.74±0.19	1.21±0.20	1.56±0.20
	30	0.43±0.06	0.58±0.11	1.16±0.37	1.83±0.28	2.91±0.20
	50	0.38±0.03	1.10±0.31	2.39±0.16	3.49±0.43	4.62±0.31
	60	0.50±0.02	1.73±0.31	2.95±0.29	4.08±0.30	4.57±0.09
	120	1.52±0.20	4.69±0.12	4.48±0.50	4.60±0.44	4.61±0.11

4.3 Revealing the influences of processing conditions

The experimental data of interfacial welding strength is first compared to the model predictions. Herein, interfacial shear strength with different welding times and soaking times are first normalized by the maximum strength (~4.6 MPa) shown in Table 1. The model predictions (from Eq. 7) are plotted in Fig. 6 as solid lines. It is observed that the established modeling framework can precisely capture the evolution of shear strength with different soaking times and welding times.

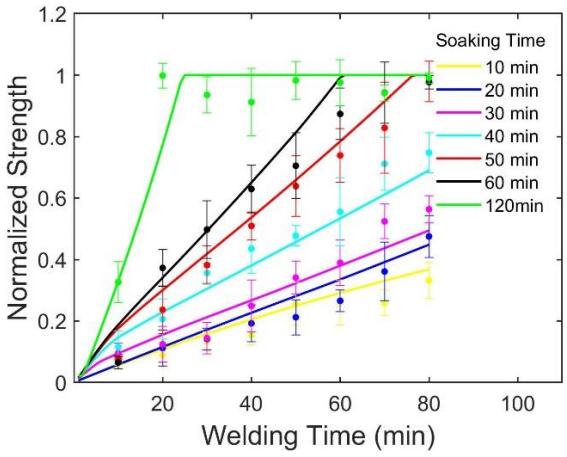

Fig. 6. The interfacial shear strength under different soaking times and welding times. Circles are the experimental data, and the solid lines are the model predictions.

With an efficient modeling framework, parametric studies are performed to reveal the influences of processing conditions, including the soaking time, welding time, welding temperature, and catalyst content in the solvent. In Fig. 7, the normalized interfacial strength is predicted with different soaking times and welding times. The applied welding temperature

is 100^{o}C. The predictions reveal how the soaking time will affect the ultimate shear strength. When the soaking time is very small (e.g., less than ~4min), the interfacial strength will increase very slowly and cannot reach the maximum value over an extended welding time (see the zoom-in view of Fig. 7). With the increment of soaking time, the evolution of shear strength can be split into three distinguished domains. i) When the soaking time is less than ~33 mins, the interfacial strength does not increase too much with the soaking time. This is due to the insufficient solvent molecules diffused into the network, leading to a lower rate of chain cleavage. The segments around the network surface are relatively long with low diffusivity, which limits their disentanglement from the network. Therefore, a higher welding time is required to promote interfacial welding strength. ii) The welding strength is substantially promoted when the soaking time is between ~33 mins and ~80 mins. This results from a gradually increased concentration of solvent molecules in the network, leading to shorter segments and faster disentanglement. iii) When the soaking time exceeds ~80 mins, the increment of shear strength becomes slow again with the soaking time. In this domain, there are excessive solvent molecules diffused into the network, which are more than enough to fully break the chains into the shortest segments. Therefore, further increasing the soaking time does not dramatically promote the welding speed. From these analyses, it is concluded that the evolution of welding strength in domains I and III is primarily dominated by the welding time, while region II is dominated by the soaking time.

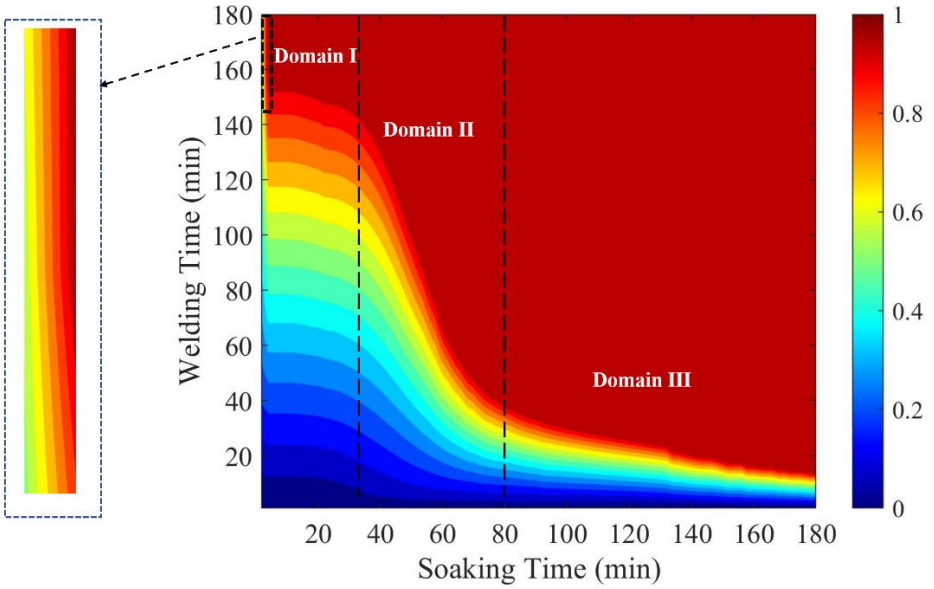

Fig. 7. The interfacial shear strength under different soaking time and welding time. The soaking temperature is 80ºC, and the welding temperature is 100ºC.

The influence of welding temperature is examined in Fig. 8, wherein the welding temperature is 100ºC, 130ºC, and 150ºC, respectively. Overall, the evolution of welding strength is still distinguished by the three domains. Increasing temperature can greatly increase the welding strength by promoting the kinetics of the three time-dependent processes, namely the chain cleavage, disentanglement, and chain connections on the interface. Therefore, at a given soaking time, a lower welding time is required to achieve an equivalent interfacial shear strength. For example, when the soaking time is ~20 mins (within Domain I), it takes ~150 mins for complete interfacial welding, while it only takes ~90mins when the temperature is increased to 150ºC.

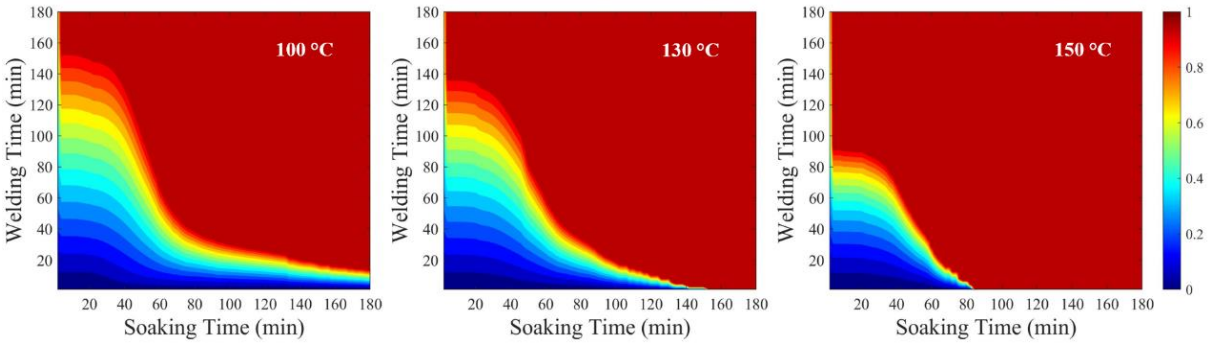

(a) **(b)** **(c)**

Fig. 8. Predictions on the interfacial shear strength at different welding temperature. The welding

temperature is **(a)** 100°C, **(b)** 130°C, and **(c)** 150°C, respectively.

The content of the BER catalyst can also affect the welding efficiency. Fig. 9 predicts the normalized welding strength with different BER energy barriers, E_a, wherein the welding temperature is 100°C. Specifically, an increasing activation energy (from Fig. 9a to Fig. 9c) suggests a decreasing amount of BER catalyst in the alcohol solvent. It is interesting to observe that when the soaking time is relatively low (in Domain I), the evolution of welding strength with the welding time does not change too much with different catalyst contents. For example, they all require ~150 mins to enable a near 100% welding degree. This is because in Domain I, the limiting factor for the welding speed is the content of diffused solvent molecules within the network. Without sufficient reactant solvent, the welding speed cannot be substantially promoted simply by increasing the catalyst content. While in Domain II with more solvent molecules diffused into the network, the role of catalyst tends to be more notable. A higher catalyst content promotes the welding process due to the increased rates of chain cleavage and connection reaction. If the catalyst is insufficient in this domain, a longer soaking time is required to allow the network to absorb more solvent molecules to achieve equivalent reaction rates, which extend the range of Domain II as shown in the figure.

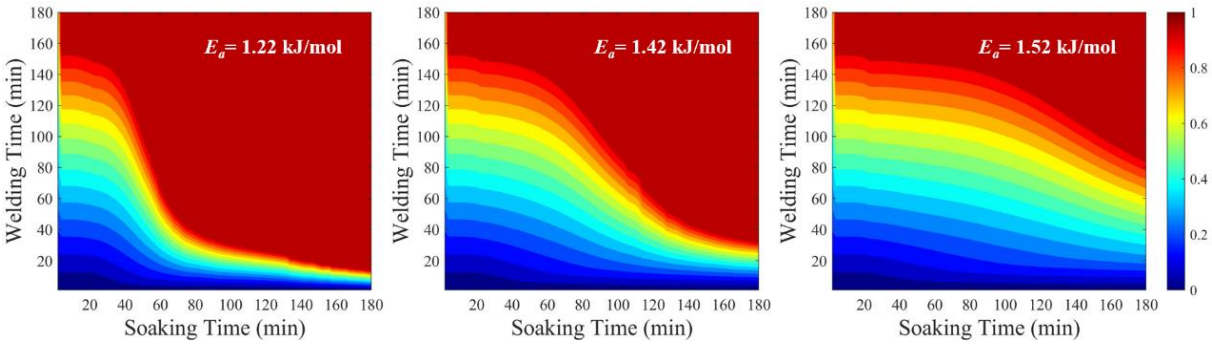

(a) **(b)** **(c)**

Fig. 9. Predictions on the interfacial shear strength with different BER energy barrier. The BER energy barrier is **(a)** 1.22 kJ/mol, **(b)** 1.42 kJ/mol, and **(c)** 1.52 kJ/mol, respectively.

4.4 Reprocessing the epoxy from powder state

The solvent-assisted interfacial welding of epoxy thermoset is applied in the microscale to reprocess the polymer wastes from the powder state. The overall reprocessing procedure is

illustrated in Fig. 10a, and the experimental images of the sample appearance are shown in Fig. 10b. The bulk polymer was first pulverized into powders. Under an optical microscope, the average particle size was estimated to be 11um ± 2um (analyzed using Image J). The powder was then soaked in the EG solvent at 80°C. After a certain amount of time, the powder was filtered out of the mixture, and the residual solvent on its surface was wiped off using paper. Under the microscope, the particles were observed to maintain the same size, which suggested no notable bulk decomposition, and the particles remained in the solid state. The powder was filled into a circular mold and then heated under pressure. After being heated for a given time, the compact powder was transformed into a transparent solid, which means that the particles were fused together in the microscale, and their interfaces disappeared.

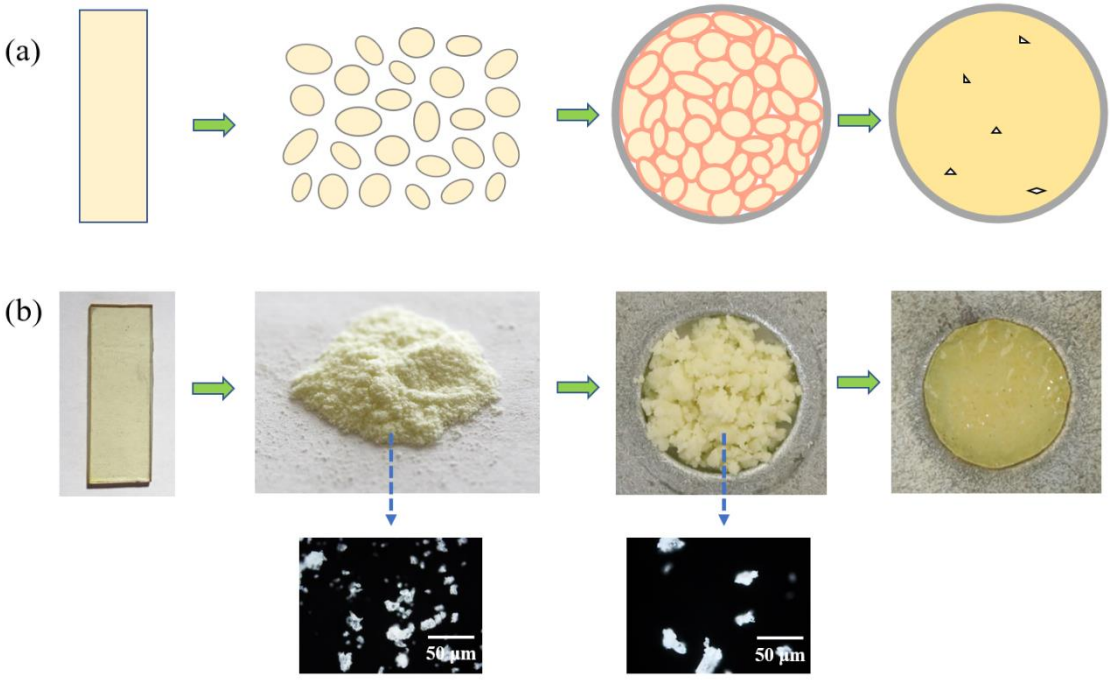

Fig. 10. The **(a)** schematic view and **(b)** experimental pictures of the epoxy sample during the reprocessing. Inset pictures in (b) show the microscopic observation of the particles using an optical microscope. The particles size is analyzed using the Image J.

The influences of powder soaking time at 80°C and welding time at 100°C on the mechanical performance of reprocessed epoxy samples are examined. Fig. 11 shows the appearance of the compact powder under the microscope with different soaking times (from bottom to top: 20 mins, 60 mins, and 120 mins, respectively) and different reprocessing times

(from left to right: 30 mins, 60 mins, 90 mins, and 120 mins, respectively). The macroscopic appearances of the reprocessed samples are also shown. For each experiment, the particles were obtained using the same grinding method, and thus, they are expected to have a similar size distribution. If the particles are not fully welded, there are numerous interfaces that exist within the sample, which are observed to be cloudy regions in the images. It can be observed from Fig. 11 that the samples gradually change from opaque to transparent as the welding time increases. As increasing the soaking time, less heating time is required for the sample to become transparent, which suggests better connectivity and faster welding of the polymer particles.

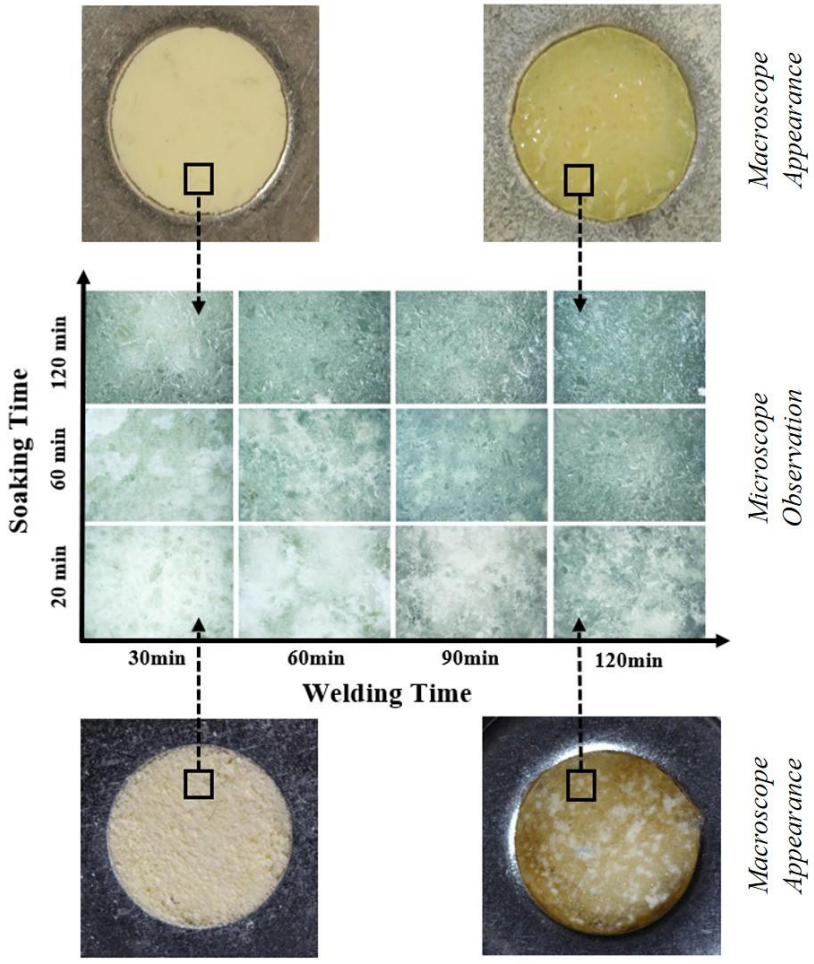

Fig. 11. The appearances of the epoxy sample when reprocessing with different soaking times and welding times.

The reprocessed epoxy samples were subject to uniaxial tension tests at room temperature to evaluate their mechanical properties. The stress-strain relationships with different soaking

times and welding times are shown in Fig. 12. For a given pre-soaking time, the modulus and ultimate strength of the reprocessed sample are observed to increase with the welding time. This is consistent with the study on the interfacial welding kinetics in Section 4.3. As the welding proceeds, more polymer chain segments diffuse onto the interface and reconnect *via* BERs, which promotes the material's mechanical strength. On the other hand, with the same welding time, a longer pre-soaking time also promotes the material's mechanical strength.

It is also interesting to observe that at the early stage of welding, the reprocessed samples are soft and stretchable, especially with an extended pre-soaking time. For example, when the soaking time is over 40 mins and welding time is 20 mins, the sample can be stretched over ~150% before fracture. This results from the incomplete solvent evaporation after heating. Different from the welding of bulk epoxy samples, the reprocessing of polymer particles was performed in a near-closed mold, which requires more time for complete solvent evaporation. While the residual solvent left in the bulk epoxy samples does not notably affect their mechanical performance, it will dramatically decrease the modulus of the reprocessed sample due to the micro size of particles and numerous interfaces involved. This also leads to the higher ultimate stretch ratio of the incompletely reprocessed samples.

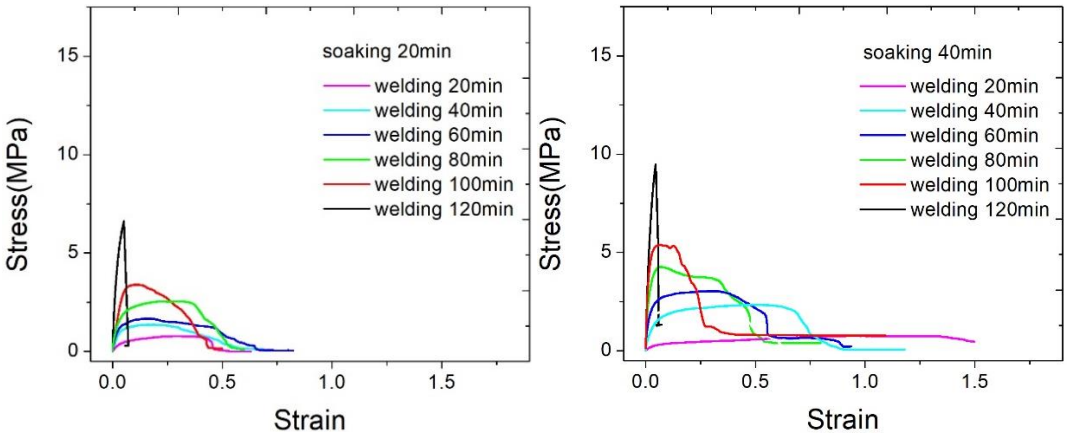

(a) **(b)**

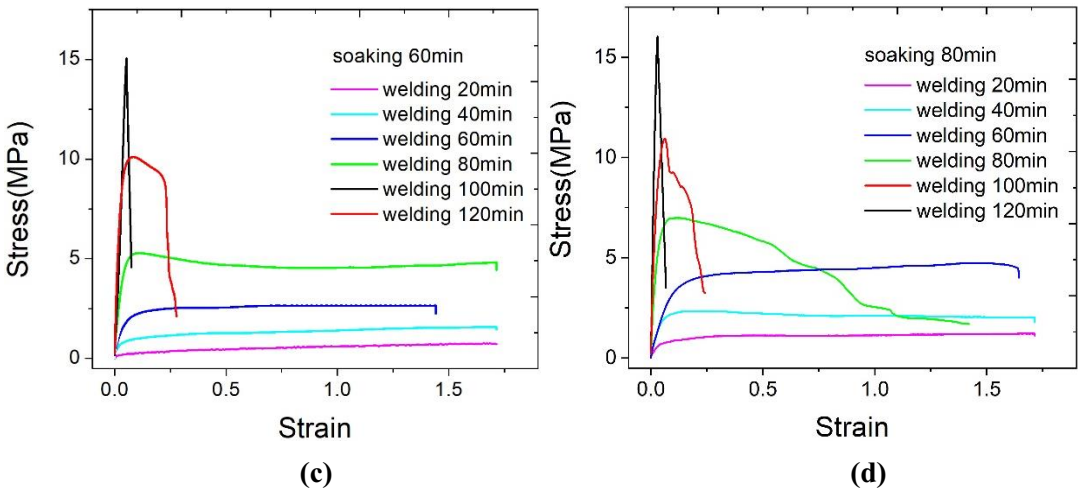

Fig. 12. Stress–strain curves of the reprocessed sample with different welding time (20, 40, 60, 80, 100, and 120 mins, respectively). The particle pre-soaking time is **(a)** 20 mins, **(b)** 40 mins, **(c)** 60 mins, **(d)** 80 mins, respectively.

The strength and failure strain of reprocessed epoxy samples are summarized in Fig. 13a and Fig. 13b with different pre-soaking times and welding times. As a control test, a fresh, unprocessed epoxy sample was subject to the uniaxial tension tests at room temperature. The measured strength (19.6 MPa) and failure strain (0.066) are marked in the figure for comparison. It is observed that with the increment of welding time, the reprocessed sample tends to be stiffer and break at lower strain amplitudes. Both material strength and failure strain gradually approach the same level of the control sample. The comparison in Fig. 13 also suggests that the particle pre-soaking time is an important parameter to control to improve reprocessing efficiency. It is observed that the evolutions of mechanical properties, especially for the strength and failure strain, are close between the soaking time of 60 mins and 80 mins. Excessively increasing the soaking time does not significantly promote the welding efficiency but may lead to the polymer particles being fully decomposed, which increases the difficulty of molding the liquid solution during heating. In addition, it may require more heating time to evaporate the solvent and thus lead to low reprocessing efficiency.

Generally, increasing soaking time or welding time can both improve the final mechanical properties of reprocessed samples. After 80 mins soaking and 120 mins welding, the strength of the reprocessed sample is 16.4 MPa, which is respectively ~83.7% of the unprocessed

control sample. The lower strength results from the micro-voids among particles after reprocessing. Herein, the porosity of the reprocessed samples is estimated by measuring the sample bulk density based on their reciprocal relationships. The volume and mass of a solid, as-fabricated epoxy sample are first measured, which determines the material density to be 1.15g/cm^3. The densities of the samples after being reprocessed at 100°C for 20 min, 40 min, 60 min, 80 min, 100 min, and 120 min (with 80 min pre-soaking time) are respectively measured. The corresponding porosities are shown in Fig. 13c. It is observed that the porosity is considerable (29.7%) at the early stage of reprocessing. It decreases to 14% after being reprocessed for 60 min and then does not dramatically decrease with the increment of time. The reason is that the individual particles cannot release internal stress, and thus are not malleable to fill the gaps among them. It is therefore concluded that the increment of the sample strength mainly results from the strength increment among particles. The porosity within the reprocessed sample is an important reason for the low strength of the re-processed sample compared to the fresh sample.

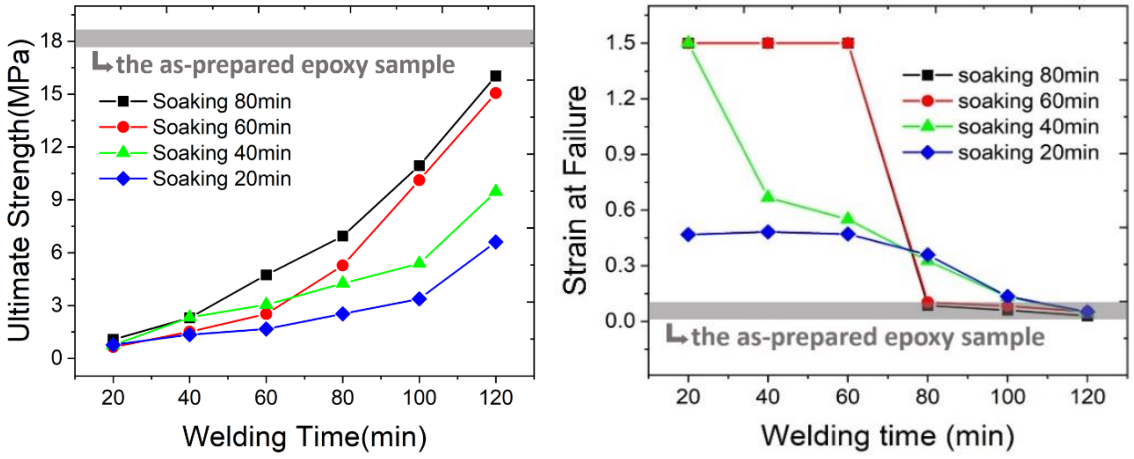

(a) **(b)**

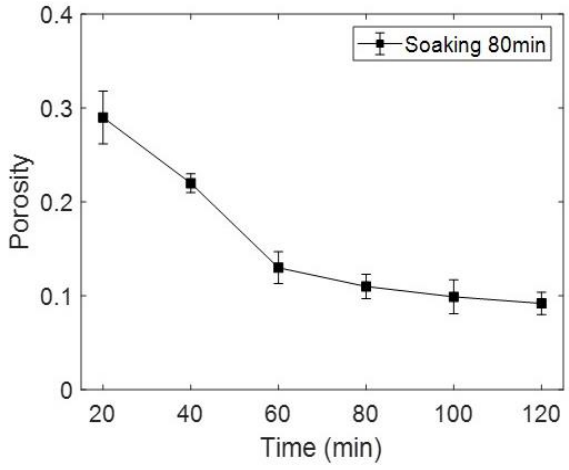

(c)

Fig. 13. (a) The ultimate strength and **(b)** failure strain of the reprocessed samples under different soaking times (20, 40, 60, 80 mins) and welding times (10, 40, 60, 80, 100, and 120 mins). **(c)** The porosity of the epoxy sample reprocessed at 80 mins soaking time and different welding times.

4. Conclusion

In this paper, an interfacial welding and reprocessing method for engineering thermosetting epoxy is developed, which is enabled by the surface depolymerization of the crosslinking networks. The welding method starts with pre-soaking the epoxy samples in an alcohol solvent mixed with the catalyst for bond exchange reactions (BERs) to allow both chemicals to diffuse into the network. During the interfacial welding, the solvent molecules will break the chains into short segments, which disentangle from the network and reconnect on the interface. The developed method leads to robust welding of engineering epoxy with covalent bonds on the interface. The study shows how the soaking time and welding time will increase the amount of connected polymer chains on the interface, and thus promote interfacial welding strength of epoxy. To assist the discussion, a multi-scale chemomechanics theoretical model is defined to capture the experimental results with different processing conditions. The parametric studies reveal welding domains that are respectively dominated by the welding time and soaking time. The model is further applied to reveal the influencing mechanisms of welding temperature and catalyst content in promoting the welding kinetics, which provide guidelines to select optimal processing conditions for the practical engineering applications of the welding method. Finally, the welding method is extended to reprocess and

recycle thermosetting epoxy from the powder state. With sufficient heating time, the reprocessed samples are shown to fully recover the mechanical properties of the unprocessed sample. Although the anhydride-cured epoxy is used as the material platform, the proposed welding and reprocessing approach can be extended to other ester-containing engineering thermosets, and thus, greatly mitigate environmental issues associated with the recycling of thermoset wastes.

Acknowledgement

K.Y. acknowledges support from the National Science Foundation (grant CMMI-1901807), USA.

Reference

1. Bower, D., *Morphology and motion.* An Introduction to Polymer Physics,(Cambridge University Press, Cambridge, 2002), 2002: p. 133-137.
2. Guo, Q., *Thermosets: structure, properties, and applications*. 2017: Woodhead Publishing.
3. Lionetto, F., et al., *Hybrid welding of carbon-fiber reinforced epoxy based composites.* Composites Part A: Applied Science and Manufacturing, 2018. **104**: p. 32-40.
4. Tsiangou, E., et al., *Ultrasonic welding of epoxy- to polyetheretherketone- based composites: Investigation on the material of the energy director and the thickness of the coupling layer.* Journal of Composite Materials, 2020. **54**(22): p. 3081-3098.
5. Perrin, H., et al., *Surface functionalization of thermoset composite for infrared hybrid welding.* Functional Composite Materials volume, 2021. **2**(10).
6. C.Ageorges and L.Ye, *Resistance welding of thermosetting composite/thermoplastic composite joints.* Composites Part A: Applied Science and Manufacturing, 2001. **32**(11): p. 1603-1612.
7. Wojtecki, R.J., M.A. Meador, and S.J. Rowan, *Using the dynamic bond to access macroscopically responsive structurally dynamic polymers.* Nature Materials, 2011. **10**(1): p. 14-27.
8. Kolomiets, E. and J.M. Lehn, *Double dynamers: molecular and supramolecular double dynamic polymers.* Chemical Communications, 2005(12): p. 1519-1521.
9. Lehn, J.M., *Dynamers: dynamic molecular and supramolecular polymers.* Progress in Polymer Science, 2005. **30**(8-9): p. 814-831.
10. Lehn, J.M., *Dynamers: Dynamic Molecular and Supramolecular Polymers.* Australian Journal of Chemistry, 2010. **63**(4): p. 611-623.
11. Skene, W.G. and J.M.P. Lehn, *Dynamers: Polyacylhydrazone reversible covalent polymers, component exchange, and constitutional diversity.* Proceedings of the National Academy of Sciences of the United States of America, 2004. **101**(22): p. 8270-8275.

12. Reutenauer, P., et al., *Room Temperature Dynamic Polymers Based on Diels–Alder Chemistry.* Chemistry – A European Journal, 2009. **15**(8): p. 1893-1900.
13. Zou, W.K., et al., *Dynamic Covalent Polymer Networks: from Old Chemistry to Modern Day Innovations.* Advanced Materials, 2017. **29**(14).
14. Jin, Y., et al., *Recent advances in dynamic covalent chemistry.* Chem. Soc. Rev., 2013. **42**(16): p. 6634-54.
15. Scott, T.F., et al., *Photoinduced plasticity in cross-linked polymers.* Science, 2005. **308**(5728): p. 1615-1617.
16. Scott, T.F., R.B. Draughon, and C.N. Bowman, *Actuation in crosslinked polymers via photoinduced stress relaxation.* Advanced Materials, 2006. **18**(16): p. 2128-2132.
17. Montarnal, D., et al., *Silica-Like Malleable Materials from Permanent Organic Networks.* Science, 2011. **334**(6058): p. 965-968.
18. Capelot, M., et al., *Metal-Catalyzed Transesterification for Healing and Assembling of Thermosets.* Journal of the American Chemical Society, 2012. **134**(18): p. 7664-7667.
19. Denissen, W., et al., *Vinylogous Urethane Vitrimers.* Adv. Funct. Mater., 2015. **25**: p. 2451–2457.
20. Denissen, W., et al., *Vinylogous Urea Vitrimers and Their Application in Fiber Reinforced Composites.* Macromolecules 2018. **51**: p. 2054–2064.
21. Zheng, N., et al., *Thermoset Shape-Memory Polyurethane with Intrinsic Plasticity Enabled by Transcarbamoylation.* . Angew. Chem. , 2016. **55**: p. 11421–11425.
22. Zheng, N., et al., *Catalyst-Free Thermoset Polyurethane with Permanent Shape Reconfigurability and Highly Tunable Triple-Shape Memory Performance.* ACS Macro Lett. , 2017. **6**: p. 326–330.
23. Obadia, M.M., et al., *Reprocessing and Recycling of Highly Cross-Linked Ion-Conducting Networks through Transalkylation Exchanges of C-N Bonds.* J. Am. Chem. Soc. , 2015. **137**: p. 6078–6083.
24. Taynton, P., et al., *Heat- or Water-Driven Malleability in a Highly Recyclable Covalent Network Polymer.* Advanced Materials, 2014. **26**(23): p. 3938-3942.
25. Taynton, P., et al., *Repairable woven carbon fiber composites with full recyclability enabled by malleable polyimine networks.* Advanced Materials, 2016. **28**(15): p. 2904-2909.
26. Luo, C., et al., *Chemomechanics in the moisture-induced malleability of polyimine-based covalent adaptable networks.* Macromolecules, 2018. **51**(23): p. 9825-9838.
27. He, X., et al., *Recyclable 3D Printing of Polyimine-Based Covalent Adaptable Network Polymers.* 3D Printing and Additive Manufacturing, 2019. **6**(1): p. 31-39.
28. He, X., et al., *A sustainable manufacturing method of thermoset composites based on covalent adaptable network polymers.* Composites Part B: Engineering, 2021. **221**: p. 109004.
29. Ponnuswamy, N., et al., *Discovery of an Organic Trefoil Knot.* Science 2012. **338**(6108): p. 783-785.
30. Li, J., et al., *Hydrogel formation upon photoinduced covalent capture of macrocycle stacks from dynamic combinatorial libraries.* Angew. Chem., Int. Ed., 2011. **50**: p. 8384-8386.

31. Podgorski, M., et al., *Toward Stimuli-Responsive Dynamic Thermosets through Continuous Development and Improvements in Covalent Adaptable Networks (CANs).* Advanced Materials, 2020. **32**(20).
32. Alabiso, W. and S. Schlögl, *The Impact of Vitrimers on the Industry of the Future: Chemistry, Properties and Sustainable Forward-Looking Applications.* Polymers, 2020. **12**: p. 1660.
33. Khan, A., N. Ahmed, and M. Rabnawaz, *Covalent Adaptable Network and Self-Healing Materials: Current Trends and Future Prospects in Sustainability.* Polymers 2020. **12**(9): p. 2027.
34. Chen, X., *A Thermally Re-mendable Cross-Linked Polymeric Material.* Science, 2002. **295**(5560): p. 1698-1702.
35. Ghosh, B. and M.W. Urban, *Induced self-repairing oxetane-substituted chitosan polyurethane networks.* Abstracts of Papers of the American Chemical Society, 2009. **238**.
36. Ghosh, B. and M.W. Urban, *Self-Repairing Oxetane-Substituted Chitosan Polyurethane Networks.* Science, 2009. **323**(5920): p. 1458-1460.
37. Imato, K., et al., *Self-Healing of Chemical Gels Cross-Linked by Diarylbibenzofuranone-Based Trigger-Free Dynamic Covalent Bonds at Room Temperature.* Angewandte Chemie-International Edition, 2012. **51**(5): p. 1138-1142.
38. Lu, Y. and Z. Guan, *Olefin Metathesis for Effective Polymer Healing via Dynamic Exchange of Strong Carbon–Carbon Double Bonds.* Journal of the American Chemical Society, 2012. **134**(34): p. 14226-14231.
39. Chen, Y.L., et al., *Multiphase design of autonomic self-healing thermoplastic elastomers.* Nature Chemistry, 2012. **4**(6): p. 467-472.
40. Cordier, P., et al., *Self-healing and thermoreversible rubber from supramolecular assembly.* Nature, 2008. **451**(7181): p. 977-980.
41. Montarnal, D., et al., *Versatile One-Pot Synthesis of Supramolecular Plastics and Self-Healing Rubbers.* Journal of the American Chemical Society, 2009. **131**(23): p. 7966-+.
42. Phadke, A., et al., *Rapid self-healing hydrogels.* Proceedings of the National Academy of Sciences of the United States of America, 2012. **109**(12): p. 4383-4388.
43. Wang, C., et al., *A Rapid and Efficient Self-Healing Thermo-Reversible Elastomer Crosslinked with Graphene Oxide.* Advanced Materials, 2013. **25**(40): p. 5785-+.
44. Das, A., et al., *Ionic Modification Turns Commercial Rubber into a Self-Healing Material.* Acs Applied Materials & Interfaces, 2015. **7**(37): p. 20623-20630.
45. Haraguchi, K., K. Uyama, and H. Tanimoto, *Self-healing in Nanocomposite Hydrogels.* Macromolecular Rapid Communications, 2011. **32**(16): p. 1253-1258.
46. Bin Ihsan, A., et al., *Self-Healing Behaviors of Tough Polyampholyte Hydrogels.* Macromolecules, 2016. **49**(11): p. 4245-4252.
47. Mayumi, K., et al., *Fracture of dual crosslink gels with permanent and transient crosslinks.* Extreme Mechanics Letters, 2016. **6**: p. 52-59.
48. He, X., D.W. Hanzon, and K. Yu, *Cyclic welding behavior of covalent adaptable network polymers.* Journal of Polymer Science Part B-Polymer Physics, 2018. **56**(5): p. 402-413.

49. Yu, K., et al., *Reprocessing and recycling of thermosetting polymers based on bond exchange reactions.* Rsc Advances, 2014. **4**(20): p. 10108-10117.
50. Yu, K., et al., *Interfacial welding of dynamic covalent network polymers.* Journal of the Mechanics and Physics of Solids, 2016. **94**: p. 1-17.
51. Liu, T., et al., *A Self-Healable High Glass Transition Temperature Bioepoxy Material Based on Vitrimer Chemistry. .* Macromolecules 2018. **51**: p. 5577–5585.
52. Giebler, M., et al., *Epoxy-Anhydride Vitrimers from Aminoglycidyl Resins with High Glass Transition Temperature and Efficient Stress Relaxation.* Polymers, 2020. **12**: p. 1148.
53. Yu, K., et al., *Reprocessing and recycling of thermoset polymers based on bond exchange reaction.* 2014.
54. Yu, K., et al., *Carbon fiber reinforced thermoset composite with near 100% recyclability.* Advanced Functional Materials, 2016. **26**(33): p. 6098-6106.
55. Yu, K., et al., *Dissolution of covalent adaptable network polymers in organic solvent.* Journal of the Mechanics and Physics of Solids, 2017. **109**: p. 78-94.
56. Shi, X., et al., *A multiscale chemomechanics theory for the solvent–assisted recycling of covalent adaptable network polymers.* Journal of the Mechanics and Physics of Solids, 2020: p. 103918.
57. Luo, C., et al., *Chemomechanics of dual-stage reprocessable thermosets.* Journal of the Mechanics and Physics of Solids, 2019. **126**: p. 168-186.
58. Shi, Q., et al., *Recyclable 3D printing of vitrimer epoxy.* Materials Horizons, 2017. **4**(4): p. 598-607.
59. Mazumdar, S., *Opportunities for Thermoset Resins in the Composites Industry.* 2008.
60. Shi, X., et al., *Primary recycling of anhydride-cured engineering epoxy using alcohol solvent.* Polymer Engineering & Science, 2019. **59**(s2): p. E111-E119.
61. Greco, A., F. Lionetto, and A. Maffezzoli, *Processing and characterization of amorphous polyethylene terephthalate fibers for the alignment of carbon nanofillers in thermosetting resins.* POLYM. COMPOS., 2015. **36**: p. 1096–1103.
62. Kuang, X., et al., *Recycling of Epoxy Thermoset and Composites via Good Solvent Assisted and Small Molecules Participated Exchange Reactions.* ACS Sustainable Chem. Eng., 2018. **6**(7): p. 9189–9197.
63. Ribas-Arino, J. and D. Marx, *Covalent Mechanochemistry: Theoretical Concepts and Computational Tools with Applications to Molecular Nanomechanics.* Chem. Rev., 2012. **112**(10): p. 5412-5487.
64. Bell, G., *Models for the specific adhesion of cells to cells.* Science, 1978. **200**(4342): p. 618-627.
65. Benjamin, A.S., et al., *Acoustic properties of Kel F-800 copolymer up to 85 GPa.* The Journal of chemical physics, 2012. **137**(1): p. 014514.
66. Stevens, L.L., et al., *Brillouin-scattering determination of the acoustic properties and their pressure dependence for three polymeric elastomers.* The Journal of chemical physics, 2007. **127**(10): p. 104906.
67. Dreger, Z., et al., *Effect of high pressure on acoustic properties of several polymers: Use of impulsive stimulated light scattering method.* Journal of Applied Physics, 2011. **109**(8): p. 083507.

68. Bower, D.I., *An introduction to polymer physics*. 2002: Cambridge ; New York: Cambridge University Press. xx, 444 p.
69. Rubinstein, M. and R.H. Colby, *Polymer physics*. 2003, New York: Oxford University Press, Oxford.
70. Chaudhury, M.K., *Rate-dependent fracture at adhesive interface.* Journal of Physical Chemistry B, 1999. **103**(31): p. 6562-6566.
71. Yu, K., et al., *Influence of Stoichiometry on the Glass Transition and Bond Exchange Reactions in Epoxy Thermoset Polymers.* RSC Advances, 2014. **4**: p. 48682-48690.
72. Luo, C., et al., *Effects of bond exchange reactions and relaxation of polymer chains on the thermomechanical behaviors of covalent adaptable network polymers.* Polymer, 2018. **153**: p. 43-51.
73. Wang, T., M.L. Dunn, and H.J. Qi, *A Computational Model for Surface Welding in Covalent Adaptable Networks Using Finite-Element Analysis.* 2016.
74. Villegas, I.F., *Ultrasonic Welding of Thermoplastic Composites.* Front. Mater., 2019 **14**: p. 6:291.

Supplementary Materials for

Interfacial welding and reprocessing of engineering thermosets based on surface depolymerization

Xiaojuan Shi[1, 2], Chaoqian Luo[1], Haibao Lu[1, *], Kai Yu[2, *]

1. National Key Laboratory of Science and Technology on Advanced Composites in Special Environments, Harbin Institute of Technology, Harbin, 150080, PR China

2. Department of Mechanical Engineering, University of Colorado Denver, Denver, CO 80217, USA

* Corresponding author HBL: luhb@hit.edu.cn; KY: kai.2.yu@ucdenver.edu

S1. Glass transition behaviors of fabricated epoxy samples

The prepared epoxy samples were subject to DMA tests to examine their thermomechanical properties, including the storage modulus and network T_g. During the DMA experiments, the samples were first stabilized at 30°C for 10 mins to reach the thermal equilibrium. Then the strain oscillated at a frequency of 1 Hz and the temperature was increased from 30°C to 85°C at a rate of 2°C min^{-1}.

To confirm the network was fully polymerized, epoxy samples were prepared with an accelerator (2,4,6-tris-dimethylaminomethyl phenol) for comparison. During the material synthesis, 100 parts by weight of epoxy monomer, 31.25 parts by weight of anhydride crosslinker, and 0.375 parts by weight of accelerator were mixed by manually stirring in a baker. After this, the mixture was placed in the vacuum to degas for 10 min and then was poured into a mold. The reactive mixture was first pre-cured at 100 °C for 2 h and then post-cured at 150 °C for another 2 h.

The glass transition behaviors of epoxy samples without and with the accelerator are shown in Fig. S1. It shows that the transition temperature T_g of the network without the accelerator (64.5ºC) is very close to that of the network with the accelerator (69.6 ºC). The network rubbery modulus, which scales to the crosslinking density, is also close to each other. The close comparison suggests that the epoxy networks used in this study are fully cured without significant unreacted or products of side reactions.

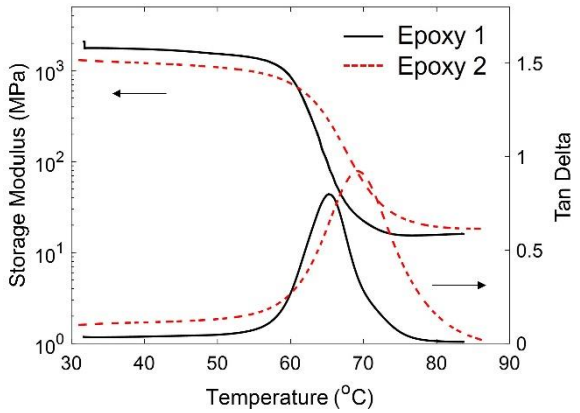

Fig. S1. Glass transition behaviors of epoxy networks without (Epoxy 1) and with (Epoxy 2) an accelerator during synthesis.

S2. Statistical analysis of segment length distribution

In the microscale, the chain segment length distribution is formulated by considering the four possible types of exchange reactions between chain segments and solvent molecules. The reactions are illustrated in Fig. S2, wherein the segments with i monomers are highlighted using dashed boxes. The mole content of segments with i monomers is denoted as C_i. In reaction (a), a segment with i monomers reacts with an EG module and splits into two shorter segments, and the mole content C_i is reduced. In reaction (b), a segment with i monomers connects with another chain segment, which generates a longer segment and a solvent molecule. The reaction also reduces the mole content C_i. In reaction (c), two short chain segments react to form a segment with i units and a solvent molecule, which increases the mole content C_i. In reaction (d), a long chain segment reacts with an EG to form a segment with i unit. The mole content C_i is also increased.

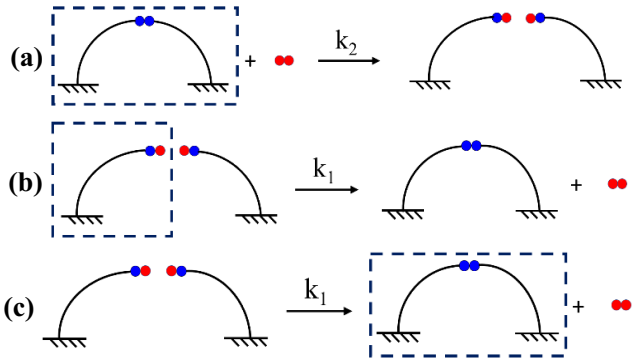

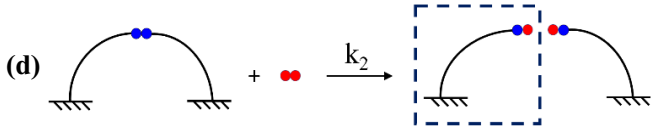

Fig. S2. Four types of exchange reactions that can change the segment length. The segment with i monomers is highlighted with dash box. The blue circles denote the exchangeable bonds on the backbone of chain segments and red circles denote the EG solvent molecule.

S3. Determination of the solvent diffusivity

The swelling test was conducted to calculate the diffusivity of EG molecules in the epoxy samples. Flat samples (30mm by 30mm) with a thickness of 1.2mm was used. The sample was soaked in ~50ml ethylene glycol solvent at different temperatures (80°C, 100°C, 120°C, and 140°C). The final soaking time was 24 hours until no notable mass increment was observed. Fig. S3a shows the mass increment of the epoxy sample as a function of SQRT (time), and Fig. S3b shows the normalized mass increase. The solid lines in these two figures are predictions from the 1D solution of the Fickian equation (see below):

$$\frac{M_t}{M_\infty} = 1 - \sum_{n=0}^{\infty} \frac{8}{(2n+1)^2 \pi^2} \exp\left(-\frac{D(2n+1)^2 \pi^2 t}{4l^2} \right), \tag{S1}$$

where M_t denotes the mass increment resulted from solvent diffusion, M_∞ is the final mass increment, l is half of the sample thickness, t is the diffusion time, and D is the diffusivity.

It can be seen that for a given temperature, a constant diffusivity is able to closely capture the experimental data, especially at the early stage of diffusion (before ~200min), wherein the mass increases linearly as a function SQRT (time). This suggests a near Fickian diffusion behavior, probably because the diffusion temperatures are highly above the network T_g, so the epoxy is in the rubbery state, not the glassy state.

After determining the diffusivities at each temperature, they are plotted in Fig. S3c (dots) as a function of inverse Kelvin temperature. The data was then used to determine the reference diffusivity D_0 and activation energy for diffusion E_{as} in Eq. 2. Using curve fitting, these two parameters are determined to be D_0=1.5×10^{-2} mm^2/s and E_{as} =26800 J/mol, respectively.

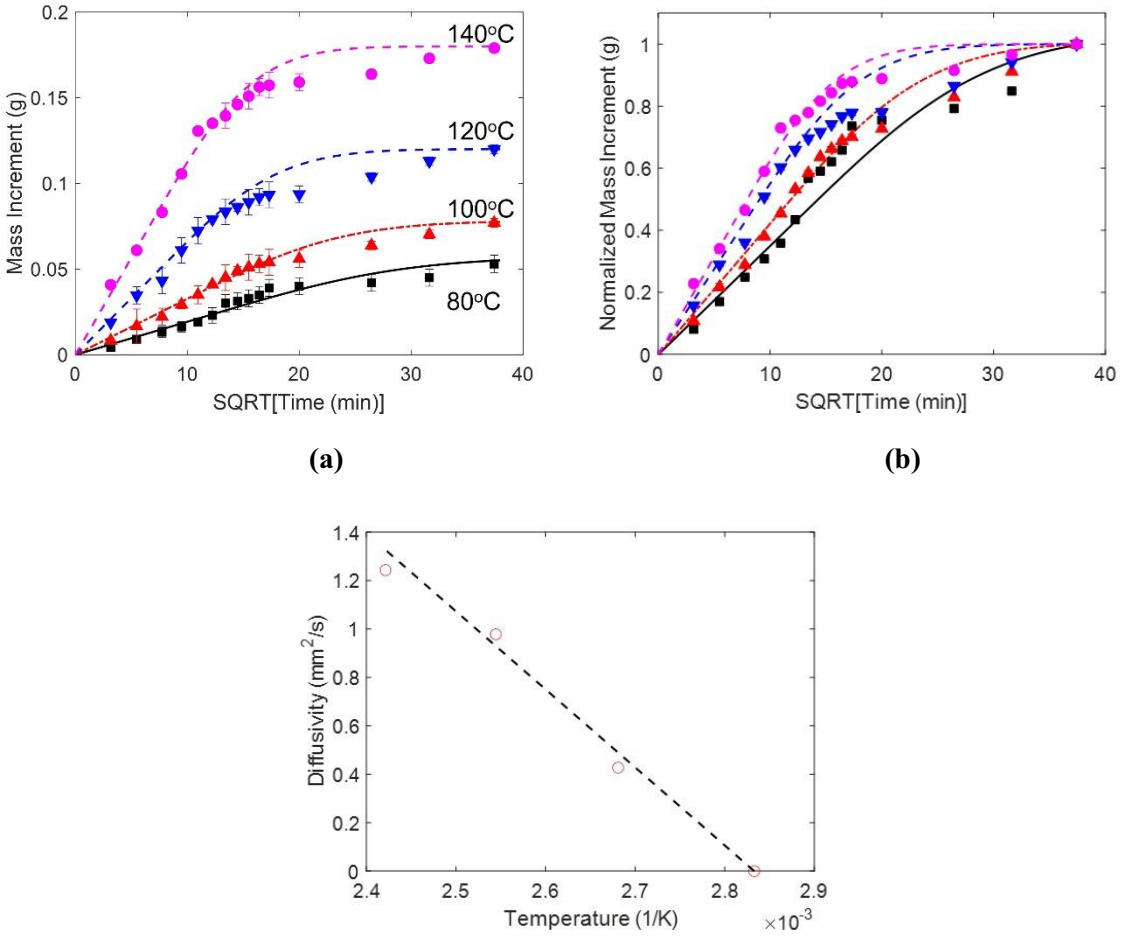

Fig. S3. (a) Mass increment as a function of square root of soaking time and temperature. Dots represent the experimental data. Solid lines represent the predictions. **(b)** Normalized mass increment as a function of square root of soaking time and temperature. **(c)** Diffusivity as a function of the inverse Kelvin temperature. The dashed line represents the prediction of Arrhenius equation.

S4. Identification of solvent evaporation rate

Gravimetric measurements were performed to characterize the evaporation rate of EG solvent at different temperatures. 10g of EG was poured in an open beaker with an evaporate area of 1256 mm^2. The mass of EG solvent was measured every 10 minutes at a series of temperatures (every 20 degrees from 120 to 220°C). Fig. S4 shows the drop of solvent mass as a function of heating time and temperature. The solvent evaporation rates are taken to be the mole loss of EG solvent per second and unit area.

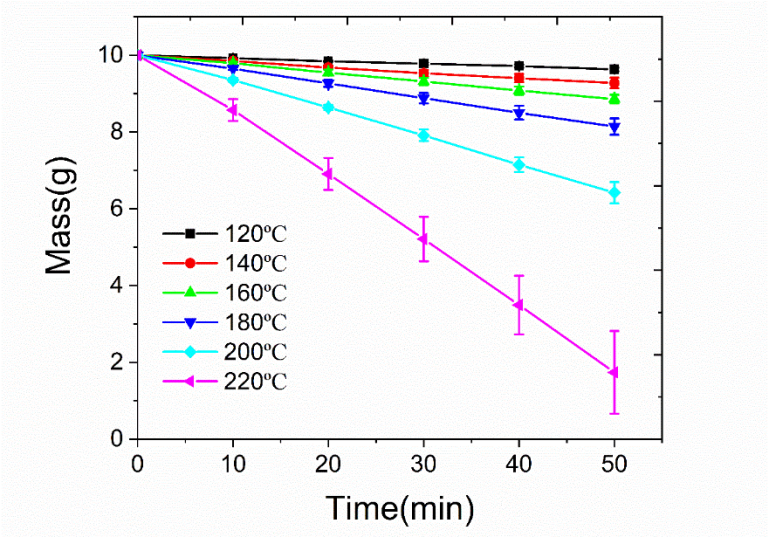

Fig. S4. The solvent mass as a function of heating time at different temperatures.

The solvent evaporation rate is summarized in Fig. S4. An exponential equation is used to describe the relationship between the evaporation rate k_d and temperature T:

$$k_d = a_1 \exp(a_2 T). \tag{S2}$$

As shown in the figure, when the fitting parameters a_1 and a_2 are set to be 1.1×10^{-5} mol/s m^2 and 0.037 °C^{-1} respectively, the proposed equation closely captures the solvent evaporation rates at different temperatures.

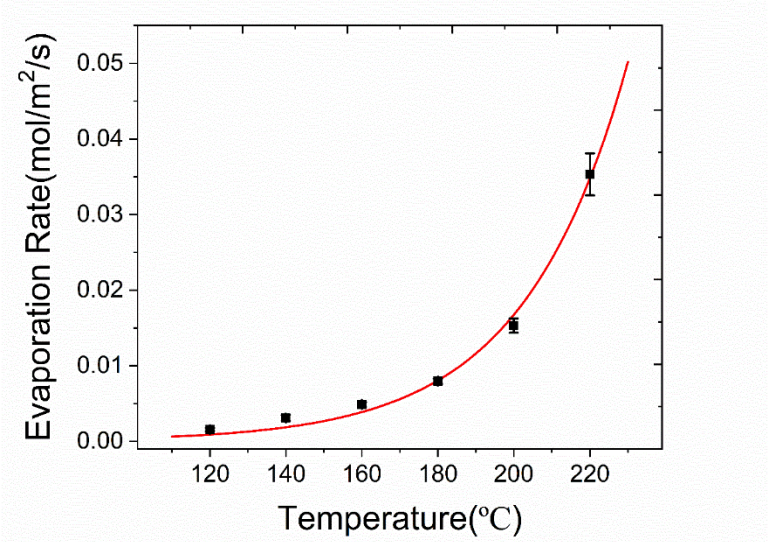

Fig. S5. The EG evaporation rate at temperature different temperatures. Dots: experimental data. Solid line: prediction.

S5. Parameters in the modeling framework

The material parameters used in the modeling framework can be calculated based on the stoichiometry during the material synthesis or measured using standard experimental tests. Herein, the average length of monomer, b, is taken to be 1 nm. In the modeling framework, N in Eq. 7 denotes the number of monomers along the chain backbone in the unprocessed epoxy sample, which can be determined by considering the monomer molecular weight and network modulus. For the precursor chemicals, epoxy monomer has a molecular weight of 1075 g/mol. The crosslinker glutaric anhydride has a molecular weight of 168 g/mol. During the synthesis, the molar ratio between the epoxide group and anhydride is 1:1, so the average molecular weight of the epoxy sample is 470 g/mol.

After synthesis, the network rubbery modulus at 150^{o}C was measured to be ~16MPa, which can be related to the molecular weight between two successive crosslinkers, M_e, as [1]:

$$G_{eq} = \rho RT / M_e, \tag{S3}$$

were G_{eq} is the shear rubbery modulus, which is taken to be one-third of the rubbery modulus under the consumption of incompressible material. ρ is the polymer density, R is the gas constant, and T is the Kelvin temperature. After calculation, the molecular weight between two successive crosslinkers is 3291 g/mol. Therefore, the amount of monomers between two crosslinkers N= (3291 g mol^{-1})/(470 g mol^{-1}) = 7.

It should be noted that when the network is fully polymerized, the chain length follows a specific distribution, rather than a fixed value. However, using existing polymer characterization techniques, it remains challenging to determine the detailed chain length distribution in the crosslinked networks. Therefore, in this study, for the convenience of analysis, we assume the uniform length of polymer chains characterized by the number N.

The BER energy barrier, E_a, determines the average time spent on a BER and the chain connection and cleavage rates. E_a was measured by performing a series of stress relaxation tests on the as-fabricated epoxy with 0.1 wt % BER catalyst at different temperatures [2, 3]. During the stress relaxation tests, the normalized relaxation modulus was used to identify the relaxation time τ_{BER}, which is taken to be the time point when the normalized relaxation modulus declines to 1/e (~36.8%). Previous studies show that τ_{BER} can be written as:

$\tau_{BER} \sim exp\ (E_a/RT)$. By fitting the experimental data, the BER energy barrier is determined to be E_a=1.22 kJ/mol.

In Eq. 4, the temperature dependency of Rouse time follows $\tau_i = \tau_0 i^2 \alpha(T)$, with τ_0 being the Rouse time of the shortest segment, and $\alpha(T)$ being the shift factor for time-temperature superposition principle (TTSP). The shift factor is written as:

$$\log_{10} \alpha(T) = -\frac{c_1(T - T_r)}{c_2 + (T - T_r)}, \tag{S4}$$

where c_1, c_2 are empirical constants. Their values were determined by performing a group of stress relaxation tests on the as-fabricated epoxy sample around its network T_g [3, 4]. Based on the TTSP, each curve is shifted to the T_g to form a master relaxation curve. The corresponding shifting factors are used to determine the fitting parameters, which are 3.7 and 21.5°C respectively.

The scaling parameter for the disentanglement rate, α_d, was determined to be 0.049. the value is determined by fitting model predictions with experimental data in Fig. 6.

All the parameters used in this model are listed in Table S1.

Table S1. Parameters in the model

Parameters	Values	Description
b	1 nm	Average length of monomer; known parameter
N	7	Amount of segments between two crosslinkers; calculated based on material stoichiometry
a_1	1.1×10^{-5} mol/s m^2	Fitting parameters for solvent evaporation rate
a_2	0.037 °C^{-1}	Fitting parameters for solvent evaporation rate
D_0	1.5×10^{-2} mm^2/s	Fitting parameters for the reference diffusivity
E_{as}	26800 J/mol	Fitting parameters for the activation energy of solvent diffusion
t_{0_BER}	2.3×10^{-2}s	Fitting parameters for a time constant of BER time
E_a	1.22 kJ/mol	Energy barrier for BER; calculated from BER-induced stress relaxation times
τ_{0s}	60 s	The Rouse time for the shortest chain segment; known parameter
c_1	3.7	Parameter of the WLF equation; calculated from the network viscoelastic relaxation times
c_2	21.5 °C	Parameter of the WLF equation; calculated from the network viscoelastic relaxation times
α_d	0.049	Fitting parameter for disentanglement rate of chain segments

S6. Stress Relaxation of Epoxy Samples

Stress relaxation tests were performed on three epoxy samples, the normalized relaxation modulus is plotted in Fig. S6. In the first test, a fresh, as-prepared epoxy sample was tested at 80°C as the reference. The network shows near-constant relaxation modulus. In the second measurement, the epoxy sample was immersed in 80°C for 20 mins, and then subject to the stress relaxation test at 80°C. It is seen that the stress relaxation is also negligible. In the third measurement, the epoxy sample was immersed in 80°C for 20 mins, and then subject to the stress relaxation test at 100°C. The network exhibits notable stress relaxation. The internal stress is dropped by ~60% within 40mins.

The notable stress relaxation is due to the BERs between the solvent molecules and epoxy networks, wherein the solvent molecules break the chain backbone and release the internal force. The comparison in Fig. S6 suggests that after soaking at 80°C, there is alcohol solvent and TBD catalyst diffused into the network, but they do not react with the network because of the relatively low temperature and inactive BERs. Most solvent molecules would isolate within the network. It is only after the temperature is increased to 100°C, the BERs between the solvent molecules and the network tends to be notable.

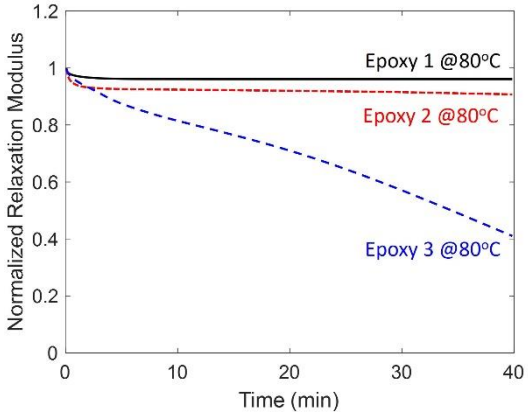

Fig. S6. Normalized relaxation modulus of Epoxy 1 (fresh, as-prepared sample), Epoxy 2, and Epoxy 3 (samples after immersed in 80°C solvent for 20 mins).

S7. Shear stress-strain relationship during the lap-shear tests.

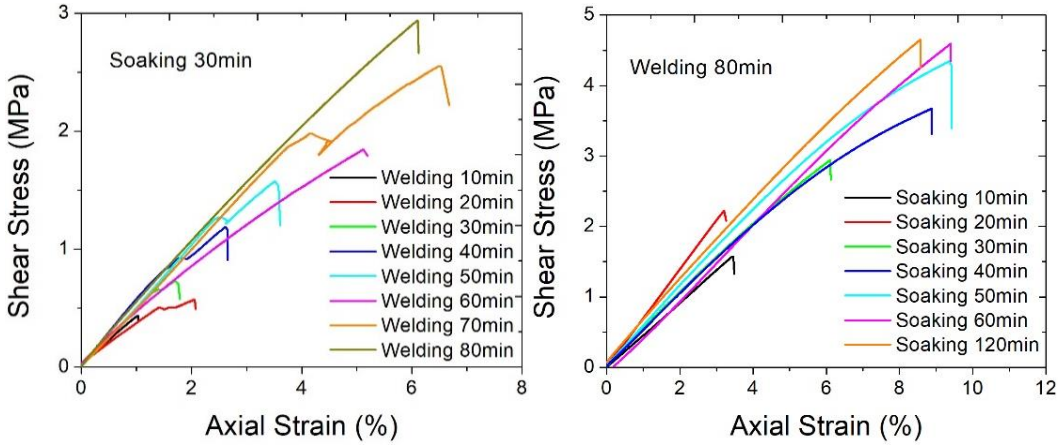

(a) **(b)**

Fig. S7. (a) The interfacial shear stress of the films welded after 30min of soaking with different welding time**. (b)** The interfacial shear stress of the films welded with different soaking time and with 80 welding time.

References:

1. Rubinstein, M. and R.H. Colby, *Polymer physics*. 2003, New York: Oxford University Press, Oxford.
2. Yu, K., et al., *Reprocessing and recycling of thermosetting polymers based on bond exchange reactions.* Rsc Advances, 2014. **4**(20): p. 10108-10117.
3. Shi, X., et al., *A multiscale chemomechanics theory for the solvent–assisted recycling of covalent adaptable network polymers.* Journal of the Mechanics and Physics of Solids, 2020: p. 103918.
4. Yu, K., Q. Ge, and H.J. Qi, *Reduced time as a unified parameter determining fixity and free recovery of shape memory polymers.* Nature communications, 2014. **5**.